Compressible *f*-plane solutions to body forces, heatings, and coolings, and application to the primary and secondary gravity waves generated by a deep convective plume

S. L. Vadas[1]

Received 19 October 2012; revised 14 January 2013; accepted 30 January 2013; published 6 May 2013.

[1] We derive the analytic, linear, *f*-plane compressible solutions to local, interval, 3-D horizontal and vertical body forces, and heat/coolings in an isothermal, unsheared, and nondissipative atmosphere. These force/heat/coolings oscillate at the frequency $\hat{a}$ and turn on and off smoothly over a finite interval in time. The solutions include a mean response, gravity waves (GWs), and acoustic waves (AWs). The excited waves span a large range of horizontal/vertical scales and frequencies ω. We find that the compressible solutions are important for GWs with vertical wavelengths $|\lambda_z| > (1 \text{ to } 2) \times \pi\mathcal{H}$ if the depth of the force/heat/cooling is greater than the density scale height $\mathcal{H}$. We calculate the primary GWs excited by a deep convective plume, ray trace them into the thermosphere, and calculate the body force/heat/coolings which result where the GWs dissipate. We find that the force/heat/cooling amplitudes are up to ∼40% smaller using the compressible (as compared to the Boussinesq) GW spectra. For a typical plume, the force/heat/coolings are deeper than $\mathcal{H}$ and have maximum amplitudes of ∼0.2 to 0.6 m/s^2 and ∼0.06 to 0.15 K/s for solar maximum to minimum, respectively. The heat/cooling consists of dipoles at z ∼150–200 km and a heating at z ∼240–260 km. We find that the compressible solutions are necessary for calculating the secondary GWs excited by these thermospheric force/heat/coolings.

Citation: Vadas, S. L. (2013), Compressible *f*-plane solutions to body forces, heatings, and coolings, and application to the primary and secondary gravity waves generated by a deep convective plume, *J. Geophys. Res. Space Physics*, *118*, 2377–2397, doi:10.1002/jgra.50163.

1. Introduction

[2] Local, interval body forces and heat/coolings can describe important fluid responses to processes such as convective overshoot, wave breaking, or wave dissipation. Here, "local" denotes a finite region in space, and "interval" denotes a finite duration in time. The responses include gravity waves (GWs), acoustic waves (AWs), and mean changes. While the temporal and spatial characteristics of the force/heat/cooling determine the wave responses, only their spatial characteristics determine the mean response [*Vadas and Fritts*, 2001] (hereafter VF01).

[3] VF01 derived the solutions to local, interval force/heat/coolings using the Boussinesq approximation. This approximation is satisfied for vertical depths of $\mathcal{D}_z \ll \mathcal{H}$. These solutions were used to calculate the primary GWs excited by deep convective plumes (modeled as vertical body forces), for example [*Vadas and Fritts*, 2009; *Vadas et al.*, 2012]. However, compressibility is expected to be important for GWs with $|\lambda_z| > (1 \text{ to } 2) \times \pi\mathcal{H}$ excited by force/heat/coolings with $\mathcal{D}_z > \mathcal{H}$.

[4] Deep convective plumes in the troposphere excite "primary" GWs and AWs [*Holton and Alexander*, 1999; *Horinouchi et al.*, 2002; *Lane et al.*, 2003; *Lastovicka*, 2006]. Because the plume updraft velocities are much less than the speed of sound, most of the energy goes into GWs rather than AWs. Most of these GWs reach nonlinear amplitudes and break, or reach critical levels, in the stratosphere and mesosphere [*Holton and Alexander*, 1999; *Lane and Sharman*, 2006]. However, some can propagate into the thermosphere [*Vadas*, 2007]. There, they eventually succumb to dissipation from kinematic viscosity, which increases exponentially with altitude [*Pitteway and Hines*, 1963; *Richmond*, 1978; *Hickey and Cole*, 1987]. This creates regions of nonzero, horizontal divergence of vertical momentum fluxes, dubbed "body forces" [*Vadas and Fritts*, 2004, 2006]. These forces are spatially and temporally localized [*Vadas and Liu*, 2013; *Vadas and Crowley*, 2010]. Heat/cooling also accompanies GW dissipation [*Walterscheid*, 1981; *Liu*, 2000; *Becker*, 2004; *Yiğit and Medvedev*, 2009], although to our knowledge, this process has not yet been calculated for the thermospheric dissipation of GWs excited by convective plumes.

[5] It is well known that local, interval force/heat/coolings excite upward and downward-propagating GWs [*Zhu and Holton*, 1987; *Vadas and Fritts*, 2001; *Vadas et al*, 2003; *Fritts et al*; 2006]. *Vadas and Liu* [2009, 2011, 2013] determined the large-scale "secondary" GWs

[1]NWRA, Boulder, Colorado, USA.

Corresponding author: S. L. Vadas, NWRA, 3380 S. Mitchell Lane, Boulder, CO 80301, USA. (vasha@nwra.com)

2169-9380/13/10.1002/jgra.50163

created by the body forces generated by GWs excited from convective plumes in Brazil using ray tracing and the Thermosphere-Ionosphere-Mesosphere-Electrodynamics General Circulation Model. These secondary GWs had horizontal wavelengths of $\lambda_H \sim$2000–5000 km and horizontal phase speeds of $c_H \sim$500–600 m/s. However, they could not resolve the secondary GWs with $\lambda_H < 2000$ km. *Vadas and Crowley* [2010] calculated the thermospheric body forces from multiple convective plumes and clusters in tropical storm Noel. These forces had variability of $\sim$100–150 km horizontally, $\sim$50–100 km vertically, and <15 min temporally. They could not calculate the excited secondary GW spectra, however, because $\mathcal{D}_z > \mathcal{H}$, causing the Boussinesq assumption to be likely inapplicable. They argued that a typical secondary GW spectrum would likely peak at horizontal wavelengths and periods of $\lambda_H \sim$100–300 km and $\tau_r < 30$ min, respectively. These scales were found to agree reasonably well with the scales of the secondary GWs observed at the bottomside of the *F* layer. Because secondary GWs can propagate to $z \sim$500–600 km [*Vadas*, 2007], can have large horizontal wind and temperature perturbations, and may play a role in seeding equatorial plasma bubbles [*Makela et al.*, 2010], it is important to model their excitation as accurately as possible in order to determine their influence on the thermosphere and ionosphere.

[6] The purpose of this paper is to generalize the VF01 and *Vadas and Fritts* [2013] solutions to include compressibility in full. As in VF01, the background is isothermal, unsheared, and nondissipative in order to obtain analytic, linear solutions. However, realistic temperature, wind, and dissipative effects can be included away from the source region via ray tracing (see section 4).

[7] We organize this paper as follows. In section 2, we derive the *f*-plane, linear, compressible solutions to temporally and spatially localized body force/heat/coolings in an isothermal, unsheared, and nondissipative fluid. In section 3, we compare the compressible and Boussinesq solutions for the GWs excited by a convective plume. In section 4, we ray trace these GWs into the thermosphere and calculate the body force/heat/coolings which result. In section 5, we determine the GWs excited by simplified force/heat/coolings in the thermosphere using the compressible and Boussinesq solutions. Section 6 contains our conclusions. Appendices contain a derivation of the energy equation, the compressible, *f*-plane polarization relations for GWs and AWs, and the initial value and special solutions.

2. Compressible Solutions to Body Forces and Heat/Coolings

[8] In this section, we derive the *f*-plane, linear, compressible solutions to horizontal and vertical body forces and heat/coolings in an isothermal, unsheared, and nondissipative fluid. Applications of these solutions include determining the GWs and AWs excited by deep convective plumes, secondary GWs excited by thermospheric body forces and heat/coolings, and GWs and AWs excited by meteor fireballs (in preparation).

2.1. Compressible, *f*-plane Fluid Equations

[9] We consider a 3-D local, interval body force or heat/cooling which turns on and off smoothly over a finite interval in time (for example, the interval can be 10–15 min, and the region can be $20^2 \times 10$ km^3 or $200^2 \times 50$ km^3 for convective overshoot and a thermospheric body force, respectively). This is a generalization of impulsive force/heat/coolings, which turn on and off instantaneously. In order to solve the equations analytically, we assume the fluid is composed of a single species and is isothermal (constant temperature), inviscid, and unsheared. We show how to include non-isothermal, dissipative, and wind effects (via ray tracing) away from the source region in section 4.

[10] The compressible momentum, mass and energy equations are

$$\frac{D\mathbf{v}}{Dt} + \frac{1}{\rho}\nabla p - \mathbf{g} + 2\mathbf{\Omega} \times \mathbf{v} = \mathbf{F}(\mathbf{x})\mathcal{F}(t), \quad (1)$$

$$\frac{D\rho}{Dt} + \rho\nabla.\mathbf{v} = 0, \quad (2)$$

$$\frac{DT}{Dt} + (\gamma - 1)T\nabla.\mathbf{v} = J(\mathbf{x})\mathcal{F}(t), \quad (3)$$

where $D/Dt = \partial/\partial t + (\mathbf{v}.\nabla)$, $\mathbf{v} = (u, v, w)$, u, v, and w are the zonal, meridional, and vertical velocities, respectively, T is temperature, ρ is density, p is pressure, $\mathbf{\Omega}$ is Earth's rotation vector, and $\mathbf{g}$ is the gravitational force. We use the ideal gas law, $p = r\rho T$, where $r = 8308/X_{MW} m^2 s^{-2} K^{-1}$, X_{MW} is the mean molecular weight of the particle in the gas, $\gamma - 1 = r/C_v$, and C_v is the mean specific heat at constant volume. The total energy equation is derived in Appendix A. The body forces and heat/coolings have time dependence $\mathcal{F}(t)$. The spatial portion of the 3-D body force is $\mathbf{F}(\mathbf{x}) = (F_x, F_y, F_z)$, and that of the heat/cooling is $J(\mathbf{x})$. Positive (negative) F_x and F_y denote an eastward (westward) and a northward (southward) forcing, respectively. Positive (negative) F_z denotes an upward (downward) forcing. Positive (negative) J denotes a heating (cooling). In our formalism, the functions $\mathbf{F}$ and J can be any arbitrary (but continuous and derivable) functions of $\mathbf{x}$.

[11] The mean molecular weight decreases from $X_{MW} = 28.9$ in the lower atmosphere to $X_{MW} = 16$ in the upper thermosphere as the molecular composition changes from primarily diatomic N_2 and O_2 to monotomic O [*Roble and Ridley*, 1994]. At the same time, γ changes from $\gamma = 1.4$ to $\gamma = 1.67$ because of the change from a diatomic to a monotomic species. The transition from diatomic to monotomic species occurs in the thermosphere at $z \sim 150$ to 300 km. In order to solve the equations analytically, we assume that X_{MW} and γ are locally constant. We show how to include variations of X_{MW} and γ away from the source region in section 4.

[12] Using the ideal gas law, we express Equation (3) in terms of the pressure:

$$\frac{Dp}{Dt} + \gamma p\nabla.\mathbf{v} = \frac{p}{T}J(\mathbf{x})\mathcal{F}(t). \quad (4)$$

We can also express Equation (3) in terms of the potential temperature θ, defined as

$$\theta = T(p_s/p)^{(\gamma-1)/\gamma}, \quad (5)$$

where p_s is the standard pressure. Then Equation (3) becomes

$$\frac{1}{\theta}\frac{D\theta}{Dt} = \frac{1}{\gamma T}J(\mathbf{x})\mathcal{F}(t). \quad (6)$$

Equation (6) expresses the well-known result that the potential temperature is conserved along the Lagrangian path of a fluid particle in a nondissipative fluid if the external heat added is zero [e.g., *Holton*, 1992]. Note that Equations (1)–(3) agree with Equations (1)–(5) in *Fritts and Alexander* [2003] (hereafter FA03).

[13] We denote the heat/cooling function we used in VF01 as J_B; that quantity was written as $J(\mathbf{x})$ on the right-hand side of Equation (2.4) in VF01 (here, the subscript B stands for Boussinesq). This function differs from the heat/cooling function we define here, $J(\mathbf{x})$. Using Equation (6), the heat/cooling defined here is related to J_B from VF01 via

$$J \simeq \frac{\gamma\mathcal{H}}{\mathrm{r}} J_B. \tag{7}$$

2.2. Linear Equations and Fourier Expansion

[14] We expand the variables as background means (overlines) plus perturbations (primes):

$$\begin{aligned} u &= \overline{U} + u', \qquad v = \overline{V} + v', \qquad w = w', \\ \rho &= \overline{\rho} + \rho', \qquad T = \overline{T} + T', \qquad p = \overline{p} + p'. \end{aligned} \tag{8}$$

We neglect the Earth's curvature, which limits wave scales to $\lambda_H < 20{,}000$–$30{,}000$ km. We also assume that the fluid obeys the f-plane approximation: $2\mathbf{\Omega} \times \mathbf{v}' \simeq f(-v'\hat{i} + u'\hat{j})$, where $f = 2\Omega \sin\Theta$ and Θ is latitude. For low-frequency waves, the f-plane approximation is a good assumption at mid-latitudes and high latitudes. At low latitudes, the so-called "beta" approximation is needed instead for low-frequency waves (note that the beta approximation is beyond the scope of this paper). For medium and high-frequency waves with periods less than a few hours, $f = 0$ is an excellent approximation at any latitude, because the Coriolis force is ineffective at such short time scales.

[15] The hydrostatic equation is $d\overline{p}/dz = -g\overline{\rho}$, yielding [*Hines*, 1960]

$$\overline{\rho} = \overline{\rho}_0 \mathrm{e}^{-z/\mathcal{H}}, \qquad \overline{p} = \overline{p}_0 \mathrm{e}^{-z/\mathcal{H}}, \tag{9}$$

where $\mathcal{H} = -\overline{\rho}(d\overline{\rho}/dz)^{-1} = \mathrm{r}\overline{T}_0/g$ is the density scale height, and $\overline{\rho}_0$, $\overline{T}_0$, and $\overline{p}_0$ are the mean density, temperature, and pressure at $z = 0$, respectively. We assume that the force/heat/cooling amplitudes are small enough that wave-mean flow and wave-wave interactions can be neglected. Linearizing Equations (1), (2), and (4), we obtain

$$\frac{\partial \mathbf{v}'}{\partial t'} + \frac{1}{\overline{\rho}}\nabla p' - \frac{\rho'}{\overline{\rho}^2}\nabla\overline{p} + f(-v'\hat{i} + u'\hat{j}) = \mathbf{F}(\mathbf{x})\mathcal{F}(t), \tag{10}$$

$$\frac{\partial \rho'}{\partial t'} + (\mathbf{v}'.\nabla)\overline{\rho} + \overline{\rho}\nabla.\mathbf{v}' = 0, \tag{11}$$

$$\frac{\partial p'}{\partial t'} + \mathbf{v}'.\nabla\overline{p} + \gamma\overline{p}\nabla.\mathbf{v}' = \frac{\overline{p}}{\overline{T}} J(\mathbf{x})\mathcal{F}(t), \tag{12}$$

where $\partial/\partial t' = (\partial/\partial t + \overline{U}\partial/\partial x + \overline{V}\partial/\partial y)$.

[16] In order for the coefficients on the left-hand sides of Equations (10)–(12) to be constant with altitude, we define the following variables:

$$\begin{aligned} &\xi = \mathrm{e}^{-z/2\mathcal{H}} u', \quad \sigma = \mathrm{e}^{-z/2\mathcal{H}} v', \qquad \eta = \mathrm{e}^{-z/2\mathcal{H}} w', \\ &\phi = \mathrm{e}^{z/2\mathcal{H}} \rho'/\overline{\rho}_0 = \mathrm{e}^{-z/2\mathcal{H}} \rho'/\overline{\rho}, \qquad \psi = \mathrm{e}^{z/2\mathcal{H}} p'/\overline{p}_0 = \mathrm{e}^{-z/2\mathcal{H}} p'/\overline{p}, \\ &\zeta = \mathrm{e}^{-z/2\mathcal{H}} T'/\overline{T}_0. \end{aligned} \tag{13}$$

We also define the scaled force/heat/coolings (denoted by the subscript "s") as

$$\begin{aligned} F_{xs} &= \mathrm{e}^{-z/2\mathcal{H}} F_x, \quad F_{ys} = \mathrm{e}^{-z/2\mathcal{H}} F_y, \\ F_{zs} &= \mathrm{e}^{-z/2\mathcal{H}} F_z, \quad J_s = \mathrm{e}^{-z/2\mathcal{H}}\, \mathrm{r}J. \end{aligned} \tag{14}$$

Because u', v', w', $\rho'/\overline{\rho}$, $p'/\overline{p}$, and $T'/\overline{T}$ increase exponentially with altitude from Equation (13), the GW and AW amplitudes increase exponentially with altitude [*Hines*, 1960].

[17] We expand ξ, σ, η, ϕ, ψ, ζ, F_{xs}, F_{ys}, F_{zs}, and J_s in a Fourier series, e.g.,

$$\xi(x,y,z,t) = \frac{1}{(2\pi)^3}\int_{-\infty}^{\infty}\int_{-\infty}^{\infty}\int_{-\infty}^{\infty} \mathrm{e}^{-i(kx+ly+mz)}\widetilde{\xi}(k,l,m,t)\mathrm{d}k\,\mathrm{d}l\,\mathrm{d}m, \tag{15}$$

where "$\sim$" denotes the Fourier transform (FT), $\mathbf{k} = (k, l, m)$ is the wavevector, and k, l, and m are the zonal, meridional, and vertical components, respectively. Equations (10)–(12) become

$$\frac{\partial\widetilde{\xi}}{\partial t''} - ik\widetilde{\psi} - f\widetilde{\sigma} = \widetilde{F_{xs}}\mathcal{F}(t), \tag{16}$$

$$\frac{\partial\widetilde{\sigma}}{\partial t''} - il\widetilde{\psi} + f\widetilde{\xi} = \widetilde{F_{ys}}\mathcal{F}(t), \tag{17}$$

$$\frac{\partial\widetilde{\eta}}{\partial t''} - im_s\widetilde{\psi} + g\widetilde{\phi} = \widetilde{F_{zs}}\mathcal{F}(t), \tag{18}$$

$$\frac{\partial\widetilde{\phi}}{\partial t''} - i\left(k\widetilde{\xi} + l\,\widetilde{\sigma} + m_s\widetilde{\eta}\right) = 0, \tag{19}$$

$$\frac{\partial\widetilde{\psi}}{\partial t''} + \delta\,\widetilde{\eta} - ic_s^2(k\widetilde{\xi} + l\,\widetilde{\sigma}) = \widetilde{J_s}\mathcal{F}(t), \tag{20}$$

where $\partial/\partial t'' = \partial/\partial t - i(k\overline{U} + l\overline{V})$, the sound speed is c_s,

$$c_s^2 = \gamma g\mathcal{H} = \gamma \mathrm{r}\overline{T}_0, \tag{21}$$

$$\delta = g(\gamma - 1) - ic_s^2 m_s, \tag{22}$$

$$m_s = m - i/2\mathcal{H}. \tag{23}$$

Since $p'/\overline{p} = \rho'/\overline{\rho} + T'/\overline{T}$, the scaled temperature perturbation is

$$\widetilde{\zeta} = \frac{\gamma}{c_s^2}\widetilde{\psi} - \widetilde{\phi}. \tag{24}$$

Table 1 shows some important symbols used in this paper.

2.3. Laplace Transform Solution Method

[18] The Laplace transform of $\widetilde{\psi}$ is as follows [*Abramowitz and Stegun*, 1972]:

$$\mathcal{L}_{\widetilde{\psi}} = \mathcal{L}(\widetilde{\psi}) = \int_0^{\infty} \mathrm{e}^{-s_r t}\widetilde{\psi}(t)\mathrm{d}t. \tag{25}$$

Therefore, $\mathcal{L}(\partial\widetilde{\psi}/\partial t) = s_r\mathcal{L}(\widetilde{\psi}) - \widetilde{\psi}(0)$, where $\widetilde{\psi}(0) = \widetilde{\psi}$ $(t = 0)$ is the initial value of $\widetilde{\psi}$. We define

$$s = s_r - i(k\overline{U} + l\overline{V}), \tag{26}$$

$$N_B^2 = (\gamma - 1)g^2/c_s^2, \tag{27}$$

$$\alpha = k\widetilde{\xi}(0) + l\,\widetilde{\sigma}(0), \qquad \beta = k\widetilde{\sigma}(0) - l\widetilde{\xi}(0), \tag{28}$$

$$A_\mathrm{F} = k\widetilde{F_{xs}} + l\widetilde{F_{ys}}, \qquad B_\mathrm{F} = k\widetilde{F_{ys}} - l\widetilde{F_{xs}}, \tag{29}$$

where N_B is the buoyancy frequency.

Table 1. Symbols and Notation Used in This Study

Symbols	Notation
$(F_x, F_y, F_z), J$	3-D body force, heating
$\mathcal{F}(t)$	temporal evolution of force/heating
$\chi, \hat{a} = 2\pi n/\chi, n$	duration, frequency, and number of cycles of force/heating
$(\xi, \sigma, \eta) = e^{-z/2\mathcal{H}}(u', v', w')$	scaled velocity perturbation
$\phi = e^{-z/2\mathcal{H}}\rho'/\overline{\rho}$	scaled density perturbation
$\psi = e^{-z/2\mathcal{H}}p'/\overline{\rho}$	scaled pressure perturbation
$\zeta = e^{-z/2\mathcal{H}}T'/\overline{T}_0$	scaled temperature perturbation
$\hat{u} = \widetilde{(e^{-z/2\mathcal{H}}u')} = \widetilde{\xi}$	FT of scaled zonal velocity perturbation
$\hat{v} = \widetilde{(e^{-z/2\mathcal{H}}v')} = \widetilde{\sigma}$	FT of scaled meridional velocity perturbation
$\hat{w} = \widetilde{(e^{-z/2\mathcal{H}}w')} = \widetilde{\eta}$	FT of scaled vertical velocity perturbation
$\hat{\rho} = \widetilde{(e^{-z/2\mathcal{H}}\rho'/\overline{\rho})} = \widetilde{\phi}$	FT of scaled density perturbation
$\hat{p} = \widetilde{(e^{-z/2\mathcal{H}}p'/\overline{\rho})} = \widetilde{\psi}$	FT of scaled pressure perturbation
$\hat{T} = \widetilde{(e^{-z/2\mathcal{H}}T'/\overline{T})} = \widetilde{\zeta}$	FT of scaled temperature perturbation
$(F_{xs}, F_{ys}, F_{zs}) = e^{-z/2\mathcal{H}}(F_x, F_y, F_z)$	scaled body force
$J_s = e^{-z/2\mathcal{H}}\mathrm{r}J$	scaled heating
$c_s = \sqrt{\gamma g\mathcal{H}} = \sqrt{\gamma \mathrm{r}\overline{T}_0}$	sound speed
$N_B = \sqrt{\gamma - 1}g/c_s$	buoyancy frequency
$(k, l, m), \omega_{Ir}, \omega_r$	wavevector, intrinsic frequency, and observed frequency
$s = i\omega_{Ir}, s_r = i\omega_r$	Laplace transform variables
$\omega_1 = \omega_{GW}, \omega_2 = \omega_{AW}$	intrinsic GW frequency, and intrinsic AW frequency
subscripts "IV", "FH"	initial value and forced/heated solutions
$\mathcal{S} = \sin\omega t + \sin\omega(\sigma - t)$	
$\mathcal{C} = \cos\omega t - \cos\omega(\sigma - t)$	

[19] We take the Laplace transform of Equations (16)–(20), then solve these equations algebraically. The resulting dispersion relation is

$$s^4 + \left[f^2 + c_s^2(\mathbf{k}^2 + 1/4\mathcal{H}^2)\right]s^2 + c_s^2\left[k_H^2N_B^2 + f^2(m^2 + 1/4\mathcal{H}^2)\right] = 0. \tag{30}$$

The two roots of Equation (30) correspond to the GW and AW, respectively:

$$s_1^2 = -\omega_1^2 = -\frac{a}{2}\left[1 - \sqrt{1 - 4b/a^2}\right], \tag{31}$$

$$s_2^2 = -\omega_2^2 = -\frac{a}{2}\left[1 + \sqrt{1 - 4b/a^2}\right], \tag{32}$$

where

$$a = -\left(s_1^2 + s_2^2\right) = \left[f^2 + c_s^2(\mathbf{k}^2 + 1/4\mathcal{H}^2)\right], \tag{33}$$

$$b = s_1^2s_2^2 = c_s^2\left[k_H^2N_B^2 + f^2(m^2 + 1/4\mathcal{H}^2)\right]. \tag{34}$$

[20] The intrinsic and ground-based wave frequencies are $\omega_{Ir} = -is$ and $\omega_r = -is_r$, respectively. Then, Equation (26) becomes the familiar expression for the Doppler shifting of a wave's frequency in a mean wind:

$$\omega_{Ir} = \omega_r - (k\overline{U} + l\overline{V}). \tag{35}$$

The intrinsic GW frequency is $\omega_{\mathrm{GW}} = \omega_1 = -is_1$, while the intrinsic AW frequency is $\omega_{\mathrm{AW}} = \omega_2 = -is_2$. Equation (30) becomes the well-known, nondissipative, acoustic-gravity wave dispersion relation first derived by *Hines* [1960] (see also Equation (22) in FA03):

$$\omega_{Ir}^4 - \left[f^2 + c_s^2(\mathbf{k}^2 + 1/4\mathcal{H}^2)\right]\omega_{Ir}^2 + c_s^2\left[k_H^2N_B^2 + f^2(m^2 + 1/4\mathcal{H}^2)\right] = 0. \tag{36}$$

For a GW which propagates much slower than the sound speed ($\omega_{\mathrm{GW}}/\sqrt{\mathbf{k}^2 + 1/4\mathcal{H}^2} \ll c_s$), the usual f-plane, anelastic GW dispersion relation is obtained from Equation (31) for $4b/a^2 \ll 1$: $s_1^2 \simeq -b/a$, or

$${\omega_{\mathrm{GW}}}^2 = \frac{k_H^2N_B^2 + f^2(m^2 + 1/4\mathcal{H}^2)}{\mathbf{k}^2 + 1/4\mathcal{H}^2} \tag{37}$$

[*Marks and Eckermann*, 1995]. The acoustic cutoff frequency ω_a is obtained from Equations (32) and (33) for $f = \mathbf{k}^2 = 0$ and $4b/a^2 \ll 1$: $\omega_a = \sqrt{a} = c_s/(2\mathcal{H})$. Since $c_s^2 = \gamma g\mathcal{H}$, $\omega_a = \gamma g/(2c_s) = [\gamma/(2\sqrt{\gamma - 1})]N_B$. For $\gamma = 1.4$ and $N_B = 0.02$ rad/s (buoyancy period of $\tau_B = 2\pi/N_B = 5.2$ min), the acoustic cutoff period is $2\pi/\omega_a = 4.7$ min.

[21] In solving the Laplace transformed equations algebraically, we also obtain the full compressible, polarization relations for GWs and AWs. These are given in Appendix B. Additionally, we derive the initial value solutions (no force/heat/coolings) in Appendix C.

2.4. Wave and Mean Responses to Interval Forces and Heat/Coolings

[22] We now derive the solution for smoothly varying, interval force/heat/coolings. The function $\mathcal{F}(t)$ is the temporal portion of the force/heat/cooling, which turns on and off smoothly for a finite interval in time. $\mathcal{F}(t)$ models realistic

body force/heat/coolings which cannot be approximated as instantaneous in time. In order to determine the solution analytically, $\mathcal{F}(t)$ must be a reasonably simple analytic function. Here, we choose $\mathcal{F}$ to be the same function as in VF01:

$$\mathcal{F}(t) = \frac{1}{\chi}\begin{cases} (1-\cos\hat{a}t) & \text{for } 0 \le t \le \chi \\ 0 & \text{for } t \le 0 \text{ and } t \ge \chi. \end{cases} \tag{38}$$

The interval forcing/heat/cooling lasts from $t = 0$ to χ and has a frequency $\hat{a}$ of

$$\hat{a} \equiv 2\pi n/\chi. \tag{39}$$

The number of cycles within this interval is $n = 1, 2, 3, \ldots$, which is a positive integer. If $n = 1$, then only a single force/heat/cooling cycle occurs over χ. An impulsive force is a special case of this more general force, and is obtained by setting $n = 1$ and $\chi \to 0$. Figure 1 shows $\mathcal{F}$ for a duration of 1 h and $n = 1, 2$, and 6. This model is more realistic than step functions or impulse functions, because the heating/forcing is gradually turned on and off smoothly over a finite duration in time.

[23] For simplicity, we set the background mean winds to zero, $\overline{U} = \overline{V} = 0$. The forced/heated solutions (denoted by the subscripts "FH") during the force/heat/cooling (i.e., when $0 \le t \le \chi$) are

$$\begin{aligned}\widetilde{\xi}_{FH}(t) = \frac{1}{\chi}\Bigg[& i\hat{a}^2 l\frac{K}{f}t + \frac{(\cos\hat{a}t-1)}{f^2-\hat{a}^2}\left\{i\hat{a}^2(kM+lfN) - f\widetilde{F_{ys}}\right\} \\ & + \frac{\hat{a}\sin\hat{a}t}{f^2-\hat{a}^2}\left\{i(-k\hat{a}^2N+lfM)+\widetilde{F_{xs}}\right\} \\ & + i\hat{a}^2\Bigg\{\frac{1}{f^2-\omega_1^2}\Bigg[(kO+lfP)(\cos\omega_1 t-1) \\ & + \left(-k\omega_1 P + \frac{lfO}{\omega_1}\right)\sin\omega_1 t\Bigg] \\ & + \frac{1}{f^2-\omega_2^2}\Bigg[(kQ+lfR)(\cos\omega_2 t-1) \\ & + \left(-k\omega_2 R + \frac{lfQ}{\omega_2}\right)\sin\omega_2 t\Bigg]\Bigg\}\Bigg],\end{aligned} \tag{40}$$

$$\begin{aligned}\widetilde{\sigma}_{FH}(t) = \frac{1}{\chi}\Bigg[& -i\hat{a}^2 k\frac{K}{f}t + \frac{(\cos\hat{a}t-1)}{f^2-\hat{a}^2}\left\{i\hat{a}^2(lM-kfN) + f\widetilde{F_{xs}}\right\} \\ & + \frac{\hat{a}\sin\hat{a}t}{f^2-\hat{a}^2}\left\{-i\left(l\hat{a}^2N+kfM\right)+\widetilde{F_{ys}}\right\} \\ & + i\hat{a}^2\Bigg\{\frac{1}{f^2-\omega_1^2}\big[(lO-kfP)(\cos\omega_1 t-1) \\ & - \left(l\omega_1 P + \frac{kfO}{\omega_1}\right)\sin\omega_1 t\Bigg] \\ & + \frac{1}{f^2-\omega_2^2}\Bigg[(lQ-kfR)(\cos\omega_2 t-1) \\ & - \left(l\omega_2 R + \frac{kfQ}{\omega_2}\right)\sin\omega_2 t\Bigg]\Bigg\}\Bigg],\end{aligned} \tag{41}$$

$$\begin{aligned}\widetilde{\eta}_{FH}(t) = \frac{1}{\chi\gamma\mathcal{H}}\Bigg[& \frac{1}{N_B^2-\hat{a}^2}\left\{\left[\hat{a}^2(i\gamma\mathcal{H}m_s-1)M-\widetilde{J_s}\right](\cos\hat{a}t-1)\right. \\ & \left. +\hat{a}\left[-\hat{a}^2(i\gamma\mathcal{H}m_s-1)N+\gamma\mathcal{H}\widetilde{F_{zs}}\right]\sin\hat{a}t\right\} \\ & + \hat{a}^2(i\gamma\mathcal{H}m_s-1)\Bigg\{\frac{1}{N_B^2-\omega_1^2}\big[O(\cos\omega_1 t-1) \\ & -P\omega_1\sin\omega_1 t\big] \\ & + \frac{1}{N_B^2-\omega_2^2}\left[Q(\cos\omega_2 t-1) - R\omega_2\sin\omega_2 t\right]\Bigg\}\Bigg],\end{aligned} \tag{42}$$

$$\begin{aligned}\widetilde{\phi}_{FH}(t) = \frac{1}{\chi c_s^2}\Bigg[& \frac{im_s g(\gamma-1)\hat{a}^2}{N_B^2}Kt \\ & - \frac{\hat{a}\sin\hat{a}t}{N_B^2-\hat{a}^2}\left\{M(\hat{a}^2 - im_s g(\gamma-1)) + \widetilde{J_s}\right\} \\ & - \frac{(\cos\hat{a}t-1)}{N_B^2-\hat{a}^2}\left\{\hat{a}^2N(\hat{a}^2-im_s g(\gamma-1)) + g(\gamma-1)\widetilde{F_{zs}}\right\} \\ & + \hat{a}^2\Bigg\{\left(\frac{im_s g(\gamma-1)-\omega_1^2}{N_B^2-\omega_1^2}\right)\left[\frac{O}{\omega_1}\sin\omega_1 t + P(\cos\omega_1 t-1)\right] \\ & + \left(\frac{im_s g(\gamma-1)-\omega_2^2}{N_B^2-\omega_2^2}\right)\left[\frac{Q}{\omega_2}\sin\omega_2 t + R(\cos\omega_2 t-1)\right]\Bigg\}\Bigg],\end{aligned} \tag{43}$$

$$\begin{aligned}\widetilde{\psi}_{FH}(t) = \frac{\hat{a}^2}{\chi}\Bigg[& Kt + \frac{M}{\hat{a}}\sin\hat{a}t + N(\cos\hat{a}t-1) \\ & + \frac{O}{\omega_1}\sin\omega_1 t + P(\cos\omega_1 t-1) \\ & + \frac{Q}{\omega_2}\sin\omega_2 t + R(\cos\omega_2 t-1)\Bigg].\end{aligned} \tag{44}$$

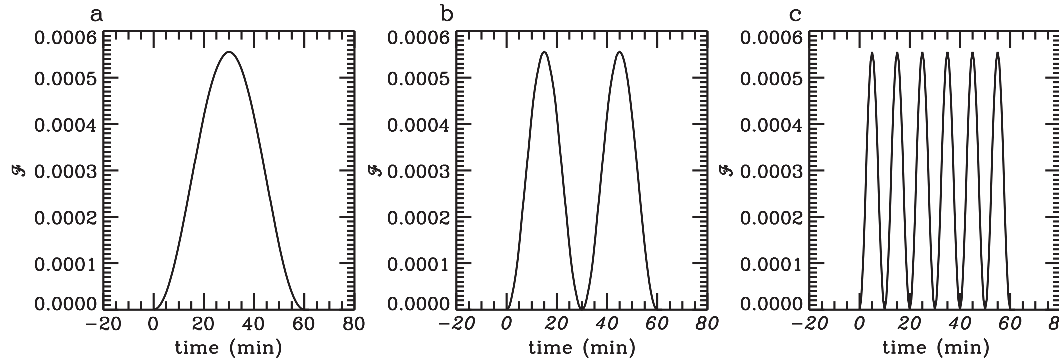

Figure 1. $\mathcal{F}(t)$ (solid) for $\chi = 1$ h; (a) $n = 1$, (b) $n = 2$, and (c) $n = 6$.

The forced/heated solutions after the force/heat/cooling is finished (i.e., when $t \geq \chi$) are

$$\widetilde{\xi}_{FH}(t) = \frac{i\hat{a}^2}{\chi}\left[l\chi\frac{K}{f} + \frac{1}{f^2-\omega_1^2}\left\{(kO + lfP)\mathcal{C}(\omega_1) + \left(-k\omega_1 P + \frac{lfO}{\omega_1}\right)\mathcal{S}(\omega_1)\right\} + \frac{1}{f^2-\omega_2^2}\left\{(kQ + lfR)\mathcal{C}(\omega_2) + \left(-k\omega_2 R + \frac{lfQ}{\omega_2}\right)\mathcal{S}(\omega_2)\right\}\right], \quad (45)$$

$$\widetilde{\sigma}_{FH}(t) = \frac{i\hat{a}^2}{\chi}\left[-k\chi\frac{K}{f} + \frac{1}{f^2-\omega_1^2}\left\{(lO - kfP)\mathcal{C}(\omega_1) - \left(l\omega_1 P + \frac{kfO}{\omega_1}\right)\mathcal{S}(\omega_1)\right\} + \frac{1}{f^2-\omega_2^2}\left\{(lQ - kfR)\mathcal{C}(\omega_2) - \left(l\omega_2 R + \frac{kfQ}{\omega_2}\right)\mathcal{S}(\omega_2)\right\}\right], \quad (46)$$

$$\widetilde{\eta}_{FH}(t) = \frac{\hat{a}^2(i\gamma\mathcal{H}m_s - 1)}{\chi\gamma\mathcal{H}}\left[\frac{1}{N_B^2-\omega_1^2}\left[O\mathcal{C}(\omega_1) - P\omega_1\mathcal{S}(\omega_1)\right] + \frac{1}{N_B^2-\omega_2^2}\left[Q\mathcal{C}(\omega_2) - R\omega_2\mathcal{S}(\omega_2)\right]\right], \quad (47)$$

$$\widetilde{\phi}_{FH}(t) = \frac{1}{\chi c_s^2}\left[\frac{im_s g(\gamma-1)\hat{a}^2}{N_B^2}K\chi + \hat{a}^2\left\{\left(\frac{im_s g(\gamma-1)-\omega_1^2}{N_B^2-\omega_1^2}\right)\left[\frac{O}{\omega_1}\mathcal{S}(\omega_1) + P\mathcal{C}(\omega_1)\right] + \left(\frac{im_s g(\gamma-1)-\omega_2^2}{N_B^2-\omega_2^2}\right)\left[\frac{Q}{\omega_2}\mathcal{S}(\omega_2) + R\mathcal{C}(\omega_2)\right]\right\}\right], \quad (48)$$

$$\widetilde{\psi}_{FH}(t) = \frac{\hat{a}^2}{\chi}\left[K\chi + \frac{O}{\omega_1}\mathcal{S}(\omega_1) + P\mathcal{C}(\omega_1) + \frac{Q}{\omega_2}\mathcal{S}(\omega_2) + R\mathcal{C}(\omega_2)\right]. \quad (49)$$

Here, we define

$$\mathcal{S}(\omega) \equiv \sin\omega t - \sin\omega(t-\chi), \quad (50)$$

$$\mathcal{C}(\omega) \equiv \cos\omega t - \cos\omega(t-\chi), \quad (51)$$

$$K = \frac{f}{\hat{a}^2 s_1^2 s_2^2}\left(ic_s^2 B_F N_B^2 + im_s g f\widetilde{J_s}\right), \quad (52)$$

$$M = \frac{1}{\hat{a}^2\left(\hat{a}^2+s_1^2\right)\left(\hat{a}^2+s_2^2\right)}\left(-ic_s^2 f B_F\left(N_B^2-\hat{a}^2\right) + \left(\hat{a}^2-f^2\right)\left(im_s g-\hat{a}^2\right)\widetilde{J_s}\right), \quad (53)$$

$$N = \frac{1}{\hat{a}^2\left(\hat{a}^2+s_1^2\right)\left(\hat{a}^2+s_2^2\right)}\left(-ic_s^2 A_F\left(N_B^2-\hat{a}^2\right) - \delta(\hat{a}^2-f^2)\widetilde{F_{zs}}\right), \quad (54)$$

$$O = \frac{1}{s_1^2\left(s_2^2-s_1^2\right)\left(\hat{a}^2+s_1^2\right)}\left(-ic_s^2 f B_F\left(N_B^2+s_1^2\right) - \left(im_s g+s_1^2\right)\left(f^2+s_1^2\right)\widetilde{J_s}\right), \quad (55)$$

$$P = \frac{1}{s_1^2\left(s_2^2-s_1^2\right)\left(\hat{a}^2+s_1^2\right)}\left(-ic_s^2 A_F\left(N_B^2+s_1^2\right) + \delta\left(f^2+s_1^2\right)\widetilde{F_{zs}}\right), \quad (56)$$

$$Q = \frac{1}{s_2^2\left(s_2^2-s_1^2\right)\left(\hat{a}^2+s_2^2\right)}\left(ic_s^2 f B_F\left(N_B^2+s_2^2\right) + \left(im_s g+s_2^2\right)\left(f^2+s_2^2\right)\widetilde{J_s}\right), \quad (57)$$

$$R = \frac{1}{s_2^2\left(s_2^2-s_1^2\right)\left(\hat{a}^2+s_2^2\right)}\left(ic_s^2 A_F\left(N_B^2+s_2^2\right) - \delta\left(f^2+s_2^2\right)\widetilde{F_{zs}}\right). \quad (58)$$

Equations (40)–(49), (24), and (13) comprise the compressible solutions in spectral (k, l, m) space. For a given time t, taking the inverse Fourier transform yields the compressible solutions in real (x, y, z) space at that time. Although these solutions are complicated, they are easily solvable numerically. Special case solutions are given in Appendix D. Eastward, westward, northward, and southward body forces excite GWs and AWs, as do heatings and coolings. Note that after the force/heat/cooling is finished, the GW and AW portions of the solution are separate and distinct; the GW terms are proportional to $\sin\omega_1 t$ and $\cos\omega_1 t$, while the AW terms are proportional to $\sin\omega_2 t$ and $\cos\omega_2 t$.

[24] We compare our solutions with VF01 and *Vadas and Fritts* [2013] in the Boussinesq limit (i.e., $\mathcal{H} \to \infty$ and $c_s^2 \to \infty$). Combining Equation (5) with the ideal gas law and linearizing, $\rho'/\overline{\rho} = (1/c_s^2)\, p'/\overline{\rho} - \theta'/\overline{\theta}$. Neglecting the pressure perturbation in the Boussinesq approximation (since it is proportional to $1/c_s^2$), we obtain the following:

$$\theta'/\overline{\theta} \simeq -\rho'/\overline{\rho}. \quad (59)$$

It is then straightforward (but tedious) to show that the compressible mean and GW solutions reduce to the Boussinesq solutions in VF01 and *Vadas and Fritts* [2013].

[25] Suppose we wish to model a physical process with a complicated temporal dependence. Because $\mathcal{F}(t) \propto \sin 2\hat{a}t$, the desired temporal dependence can be obtained by summing the solutions for many $\mathcal{F}(t)$ functions with various values of $\hat{a}$, as was done in VF01.

3. High-frequency GWs Excited by a Single Convective Plume

[26] Over the past few decades, many numerical models have been developed to simulate the GWs excited by deep convection [*Holton and Alexander*, 1999; *Pandya and Alexander*, 1999; *Horinouchi et al.*, 2002; *Lane et al.*, 2003]. Within a moist convective system, both diabatic forcings and nonlinear forcings excite GWs [*Lane et al.*, 2001]. Since these sources are largely out of phase, linear "dry-air" models including only one source must reduce the GW amplitudes by $\sim$2 [*Song et al.*, 2003; *Choi et al.*, 2007]. With this reduction and the condition that only GWs with $c_H > 20$–25 m/s be included, the modeled GWs excited by a convective plume may be represented by either a diabatic forcing or a nonlinear forcing. Some dry-air models implement diabatic forcing [*Alexander et al.*, 1995; *Piani et al.*, 2000; *Walterscheid et al.*, 2001; *Beres*, 2004], while others model the forcing due to the overshooting of a convective plume [*Stull*, 1976; *Vadas and Fritts*, 2009]. GW excitation from deep convection excites high-frequency GWs with $\lambda_H \sim 1$ km to hundreds of kilometers and with periods of 5 min to a few hours.

[27] Our convective plume model implements the latter process by calculating the idealized motion of the fluid

within a plume via a vertical body force [*Vadas and Fritts*, 2009]. This model neglects moisture processes and solves the linear equations in a locally unsheared environment with a constant buoyancy frequency. This vertical body force creates the acceleration needed to push the fluid in the plume from the troposphere into the lower stratosphere (convective overshoot). This overshoot pushes the stratospheric air upwards, after which gravity pulls it back downward because the air is stably stratified. This movement excites AWs and GWs. Observations and simulations show that there are typically many small updrafts within the "envelope" of a convectively unstable region, which give rise to GW spectra concentrated at small scales of ∼5–10 km [*Larsen et al.*, 1982; *Alexander et al.*, 1995; *Lane et al.*, 2003; *Lane and Knievel*, 2005]. Our model neglects these individual updrafts and therefore does not include the very small-scale GWs which tend to break, reach critical levels, or reflect in the stratosphere. Instead, our model calculates the spectrum of "larger-scale" GWs excited by the "envelope" of the upward motion of air within the coherently moving small updrafts. These GWs are small to medium-scale with c_H > 20–25 m/s. Our model is therefore appropriate for mesosphere and thermosphere GW studies.

[28] Each vertical body force is modeled as a Gaussian in space, is centered at $x = x_0$, $y = y_0$, and $z = z_0$, and is described by its geometry (horizontal width and vertical depth), duration, maximum (vertical) updraft velocity, location, and time of occurrence. In order to take into account ground reflection, we also include an identical "image" force at $x = x_0$, $y = y_0$, and $z = -z_0$ [*Vadas and Fritts*, 2009]:

$$F_z = F_0 \exp\left(-\frac{(x-x_0)^2}{2\sigma_x^2} - \frac{(y-y_0)^2}{2\sigma_y^2}\right)\left[\exp\left(-\frac{(z-z_0)^2}{2\sigma_z^2}\right) - \exp\left(-\frac{(z+z_0)^2}{2\sigma_z^2}\right)\right]. \tag{60}$$

The top of the body force, located at $z \sim z_0 + 2.25\sigma_z$, is typically set to be 1–2 km above the tropopause, in order to account for convective overshoot. The plume location, time of occurrence, width, maximum updraft velocity, and tropopause altitude are determined in practice from satellite images and Convective Available Potential Energy (CAPE) and tropopause maps [e.g., *Vadas and Liu*, 2009; *Vadas and Crowley*, 2010]. We determine F_0 by calculating the body force solution numerically in time and linearly scaling by the maximum updraft velocity. The "best-fit" plume duration and depth have been determined primarily via comparison of the model results with the amplitudes and parameters of concentric GWs from convective plumes as observed in the OH airglow near the mesopause [*Vadas et al*., 2009a, b, 2012]. The best-fit depth and duration have been found to be ∼10 km and $\chi \sim 10$ min, respectively. This duration is consistent with high-time-resolution NEXRAD data, which found that a new plume within a thunderstorm typically appears every 15–20 min [*Vadas et al.*, 2012]. Note that this 15–20 min time period includes the growth and collapse of the plume plus the time for the formation of a new plume.

[29] We also utilize our anelastic, dissipative GW ray trace model, which propagates the excited GWs (with their phases) into the mesosphere and thermosphere and reconstructs the GW fields there [*Vadas et al.*, 2012]. This model includes realistic wind and temperatures as well as thermospheric dissipation for high-frequency GWs. It can also include GW saturation, although we do not include this here, in order to more easily interpret the results. Further details of both models can be found in *Vadas et al.* [2012].

[30] Because convective plumes only excite medium and high-frequency GWs, the Coriolis force is not important; therefore, we can set $f = 0$ for calculating their amplitudes (recall from Section 2.2 that $f = 0$ is an excellent approximation for medium and high-frequency GWs at any latitude). In this limit, the compressible solutions derived in section 2 simplify considerably. The postforcing ($t \geq \chi$), compressible zonal, and vertical velocity perturbations resulting from a vertical body force with $f = 0$ (using Equations (45), (47), (13), and (14)) are

$$\left(\widetilde{e^{-z/2\mathcal{H}}u'}\right) = \frac{km\omega_1^2}{k_H^2N_B^2}\left[\frac{1+i\left(\frac{\gamma-2}{2\gamma\mathcal{H}m}\right)}{1-\omega_1^2/\omega_2^2}\right]\left(\widetilde{e^{-z/2\mathcal{H}}F_z}\right)\left\{-\frac{\hat{a}^2\mathcal{S}(\omega_1)}{\chi\omega_1\left(\hat{a}^2-\omega_1^2\right)}+\frac{\hat{a}^2\mathcal{S}(\omega_2)}{\chi\omega_2\left(\hat{a}^2-\omega_2^2\right)}\right\}, \tag{61}$$

$$\left(\widetilde{e^{-z/2\mathcal{H}}w'}\right) = \frac{m^2\omega_1^2}{k_H^2N_B^2}\left[\frac{1+\left(\frac{\gamma-2}{2\gamma\mathcal{H}m}\right)^2}{1-\omega_1^2/\omega_2^2}\right]\frac{\hat{a}^2}{\chi}\left(\widetilde{e^{-z/2\mathcal{H}}F_z}\right)\left\{\frac{\omega_1\mathcal{S}(\omega_1)}{\left(N_B^2-\omega_1^2\right)\left(\hat{a}^2-\omega_1^2\right)}-\frac{\omega_2\mathcal{S}(\omega_2)}{\left(N_B^2-\omega_2^2\right)\left(\hat{a}^2-\omega_2^2\right)}\right\}. \tag{62}$$

Here, each widetilde " $\sim$ " encompasses the Fourier transform of all factors within the enclosed parenthesis. Those terms proportional to $\mathcal{S}(\omega_1)$ and $\mathcal{C}(\omega_1)$ are the GW solutions, while those terms proportional to $\mathcal{S}(\omega_2)$ and $\mathcal{C}(\omega_2)$ are the AW solutions. Note that the vertical body force is multiplied by $\exp(-z/2\mathcal{H})$ before applying the Fourier transform. We compare this solution to the simpler Boussinesq solution, remembering that the Boussinesq approximation is valid for force vertical depths less than $\mathcal{H}$ or $|\lambda_z| << 4\pi\mathcal{H}$. From VF01, the postforcing ($t \geq \chi$) Boussinesq zonal and vertical velocity perturbations resulting from a vertical body force are as follows:

$$\widetilde{u'} = -\frac{km}{k_H^2}\frac{\omega_1^2}{N_B^2}\frac{\hat{a}^2}{\chi\omega_1\left(\hat{a}^2-\omega_1^2\right)}\widetilde{F_z}\mathcal{S}(\omega_1), \tag{63}$$

$$\widetilde{w'} = \left(\frac{\omega_1}{N_B}\right)^2\frac{\hat{a}^2}{\chi\omega_1\left(\hat{a}^2-\omega_1^2\right)}\widetilde{F_z}\mathcal{S}(\omega_1). \tag{64}$$

In the Boussinesq limit, for which $m^2\omega_1^2/\left[k_H^2\left(N_B^2-\omega_1^2\right)\right] \simeq 1$, $\omega_1^2 \ll \omega_2^2$, $\mathcal{H} \to \infty$, and $c_s^2 \to \infty$, it is easy to show that Equations (61) and (62) reduce to Equations (63) and (64).

[31] Figure 2 shows contours of ω_1^2/ω_2^2 for a buoyancy period of $\tau_B = 2\pi/N_B = 5.2$ min. We see that $\omega_1^2/\omega_2^2 \leq 0.25$, even for very large c_H. Therefore, there are likely only small changes in the GW compressible amplitudes due to the $[1-\omega_1^2/\omega_2^2]$ factors in Equations (61) and (62). However, the factors in the numerators of the square brackets are expected to be important for $|m|\mathcal{H} <$ few or $|\lambda_z| > \pi\mathcal{H}$.

[32] While the AW and GW amplitudes are similar for impulsive forcings, the AW amplitudes are suppressed by $(2\pi n)^{-1}\hat{a}^3/\omega_2^3$ from their impulsive values for forces with $2\pi/\hat{a} \gg \tau_B$. For these slow forcings, the amplitudes of high-frequency GWs with intrinsic periods of

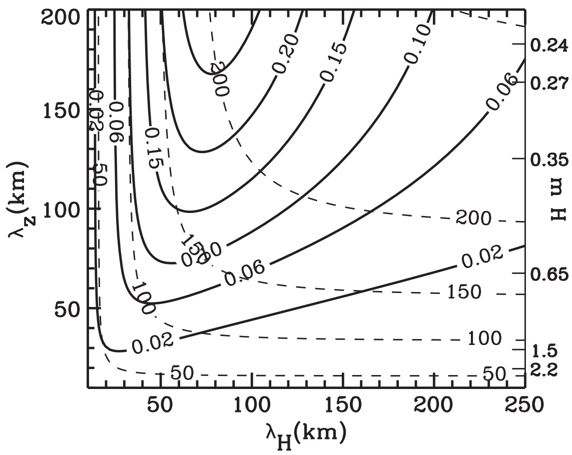

Figure 2. Contour plot showing $(\omega_1/\omega_2)^2$ (solid) for N_B = 0.02 rad/s, γ = 1.4, g = 9.8 m/s^2, c_s = 310 m/s, and $\mathcal{H}$ = 7 km. The right-hand y axis shows the corresponding values of $m\mathcal{H}$. Dashed lines show c_H in intervals of 50 m/s.

$\tau_{Ir} < \pi/\hat{a}$ are significantly reduced, where $\tau_{Ir} = 2\pi/\omega_{Ir}$. This is because the GWs oscillate faster than the forcing frequency.

[33] We model a single convective plume with a diameter of $\mathcal{D}_H = 4.5\sigma_x = 4.5\sigma_y$ = 20 km, a depth of $\mathcal{D}_z = 4.5\sigma_z$ = 10 km, and a duration of χ = 10 min. Note that D_z is somewhat larger than $\mathcal{H}$ = 7 km. We also choose a tropopause altitude of z_{trop} = 14 km and an overshoot depth of 1 km. We locate the "top" of the body force at z = 15 km and the center at z_0 = 10 km. We also choose F_0 = 600 m/s, as this results in a maximum updraft velocity of w_{pl} = 35 m/s. These values are typical for plumes within thunderstorms. Note that the estimated average time taken for a fluid parcel to move upward the depth of the plume is $\sim \mathcal{D}_z/(w_{\mathrm{pl}}/2) \sim$ 10 min. We assume typical lower atmospheric parameters of $\mathcal{H}$ = 7 km, $\underline{N_B}$ = 0.02 rad/s, γ = 1.4, $\mathrm{X_{MW}}$ = 30, g = 9.8 m/s^2, and $\overline{T}$ = 246 K. Additionally, we set $\overline{U} = \overline{V} = 0$. We also set $f = 0$ because a convective plume excites primarily medium and high-frequency GWs. For illustration purposes, we also consider a somewhat shorter (less realistic) plume duration of χ = 8 min.

[34] Figures 3a and 3b show the Boussinesq and compressible vertical flux of zonal momentum spectra for GWs with $l = 0$ [Equation(35) from *Vadas and Fritts* [2009]]:

$$km\left(2|\overline{\widetilde{u'}\widetilde{w'}^*}|\Delta k\Delta l\Delta m\right), \qquad km\left(2|\overline{\widetilde{\xi}\widetilde{\eta}^*}|\Delta k\Delta l\Delta m\right), \tag{65}$$

respectively. Here, Δk, Δl, and Δm are the spectral grid spacings of the FT used to calculate the spectral solutions [Equation (16) from *Vadas and Fritts* [2009]]:

$$\Delta k = \frac{2\pi}{L_x}, \Delta l = \frac{2\pi}{L_y}, \Delta m = \frac{2\pi}{L_z}, \tag{66}$$

where L_x, L_y, and L_z are the x, y, and z domain lengths, respectively. Because of ground reflection, each spectrum has two peaks. The peaks occur at $\lambda_H \sim 20-60$ km, $|\lambda_z| \sim 10-40$ km, and $\tau_{Ir} \sim 8-15$ min. Increasing the force duration from 8 to 10 min shifts the GW spectrum to larger periods and larger λ_H and decreases the peak of the spectrum by a factor of $\sim$2. We see that the Boussinesq and compressible spectra are similar for a given χ. We show the fractional difference for χ = 10 min in Figure 3c. In general, the compressible and Boussinesq solutions differ for GWs with $|\lambda_z| > (1 \text{ to } 2) \times \pi\mathcal{H}$. For periods $\tau_{Ir} > 8$ min and $|\lambda_z| > 40$ km (i.e., $|\lambda_z| > 2\pi\mathcal{H}$ = 44 km), the Boussinesq amplitudes are 20–100% larger. For $\tau_{Ir} < 8$ min, the compressible amplitudes are 20–40% larger. However, because

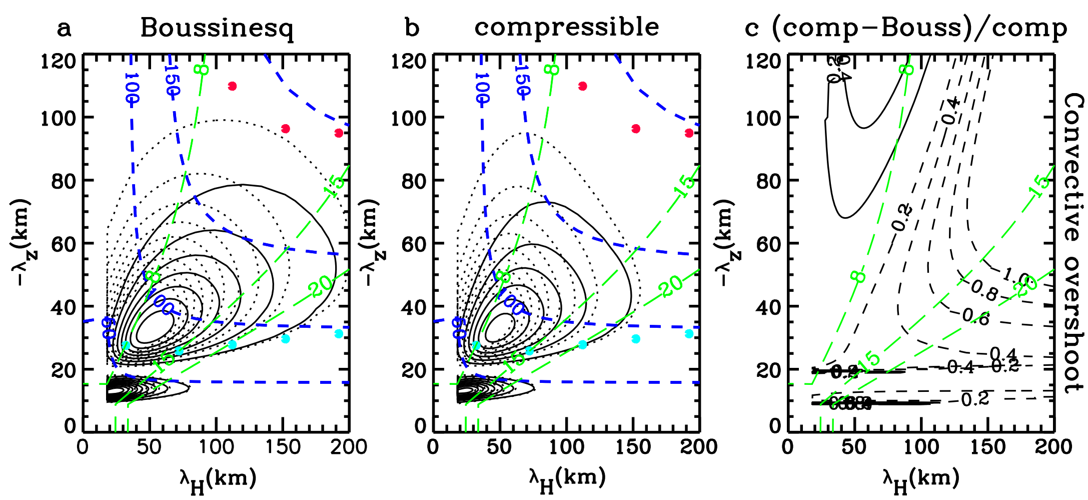

Figure 3. (a) Boussinesq and (b) compressible vertical flux of zonal momentum for the GWs excited by a convective plume with $\mathcal{D}_H$ = 20 km and χ = 10 min (solid) and χ = 8 min (dotted). (c) (Compressible–Boussinesq)/compressible fluxes from Figures 3a and 3b for χ = 10 min. Solid (dashed) lines show positive (negative) values. The turquoise and red dots in Figures 3a and 3b indicate GWs with select λ_H for which z_{diss} = 150 km and 220 km, respectively. Blue short-dashed lines indicate the intrinsic horizontal phase speed c_{IH} in 50 ms^{-1} intervals. The green long-dashed lines show GW intrinsic periods of τ_{Ir} = 8, 15, and 20 min.

these amplitudes are quite small, and because GWs with $\tau_{Ir} < 8$ min reflect downward in the lower thermosphere (since $\tau_B > 8$ min there), we do not expect the latter difference to be significant in the thermosphere. Because the GWs responsible for creating body forces in the thermosphere have τ_{Ir} = 10–20 min and $|\lambda_z| \sim$ 40–50 km [*Vadas and Liu*, 2009], including compressibility is expected to reduce the body force amplitudes by $0.4^2 - 0.6^2 \sim$20–40% if the GWs do not saturate. Here, the body force amplitude is proportional to the GW amplitude squared. We calculate the body forces for both spectra in section 4.

[35] We define $z_{\rm diss}$ to be the altitude where a GW's momentum flux is maximum. At this altitude, the following expression is approximately satisfied [*Vadas and Liu*, 2009]:

$$\frac{\lambda_z^3 \omega_{Ir}}{8\pi^3 \mathcal{H}(1+\mathrm{Pr}^{-1})} \sim \nu. \tag{67}$$

[36] For select values of λ_H, we show in Figures 3a and 3b the GWs at $z_{\rm diss}$ = 150 km. Here, we solve Equation (67) iteratively for m given a λ_H. We use typical values $N_B = 1.9 \times 10^{-2}$ rad/s, $\mathcal{H}$ = 17 km, and $\nu = 1 \times 10^4$ m^2/s. Those GWs far below an imaginary line connecting these dots dissipate below this altitude, while those GWs above this imaginary line propagate above this altitude. We also show $z_{\rm diss}$ = 220 km. Here, we use $N_B = 1.4 \times 10^{-2}$ rad/s, $\mathcal{H}$ = 31 km, and $\nu = 2 \times 10^5$ m^2/s. While most of the GWs with $c_H > 75$ m/s survive to $z \sim 150$ km, only those with $c_H > 180$ m/s survive to $z \sim 220$ km. This statement, however, assumes that the winds are zero. Because the winds in the thermosphere can be quite large, it is possible for some primary GWs to propagate opposite to the background winds to $z > 250$ km (see section 4). However, it is unlikely that a primary convective GW will propagate to $z \sim 400$ km, unless it has an intrinsic frequency quite close to the buoyancy frequency [*Earle et al.*, 2008; *Vadas*, 2007].

[37] In Figure 4, we show the GW temperature perturbations for the exact compressible (solid) and Boussinesq (dotted) solutions at z = 70 km and y = 0 for various times. These solutions are obtained by taking the inverse Fourier transform of the spectral (k, l, m) solutions. The agreement is quite good for small to medium-horizontal-scale GWs, showing that the Boussinesq solutions are excellent for mesospheric studies of convective GWs.

[38] Because of the isothermal, unsheared, and nondissipative assumptions used to derive the Fourier-Laplace (exact) solutions, these solutions are not very useful in (x, y, z) space. However, they are useful in (k, l, m) space for defining the initial GW spectra. Then, we can ray trace these spectra through realistic atmospheres with varying temperature, wind, and dissipation [*Vadas and Crowley*, 2010; *Vadas et al.*, 2009a, b, 2012; *Vadas and Liu*, 2009, 2013]. In order to test the ray trace model, we ray trace the compressible GW spectrum from the center of the aboveground vertical body force (i.e., at $x = y = 0$, z = 10 km) and at $t = \chi/2$ = 5 min through the isothermal, nondissipative atmosphere. Ground reflections are not allowed. The cell sizes within this domain (for reconstruction of the GW field near the mesopause) are 6 km × 6 km × 3 km × 4 min in x, y, z, and t, respectively. We reconstruct the GW field using the formalism described in *Vadas and Fritts* [2009]. The reconstructed solutions are shown as dashed lines in Figure 4. In general, the agreement between the ray trace and Fourier-Laplace solutions is quite good. Differences occur at large radii where there are less GWs within the spectrum [*Vadas and Fritts*, 2009]. The solutions agree somewhat less well for small radii because of the finite plume width. There are also differences at t = 58 min. This likely occurs because the slower ground-reflected GWs are reaching this altitude in the exact solutions.

4. Thermospheric Body Force/Heat/Coolings From a Convective Plume

[39] As GWs propagate into the thermosphere, they are eventually dissipated by molecular viscosity. Those GWs having the largest $|\lambda_z|$ (typically achieved for those GWs propagating against the background wind) reach the highest altitudes before dissipating [*Vadas*, 2007; *Fritts and Vadas*, 2008]. As these GWs dissipate, they create thermospheric body forces in the direction of propagation, which accelerate the background wind in that direction [*Vadas and Fritts*, 2004, 2006; *Vadas and Liu*, 2009, 2011, 2013; *Vadas and Crowley*, 2010]. They also heat/cool the fluid [*Walterscheid*, 1981; *Liu*, 2000; *Becker*, 2004; *Yiğit and Medvedev*, 2009]. Previous work with convective plumes has only considered the effect body forces have on the thermosphere; to our

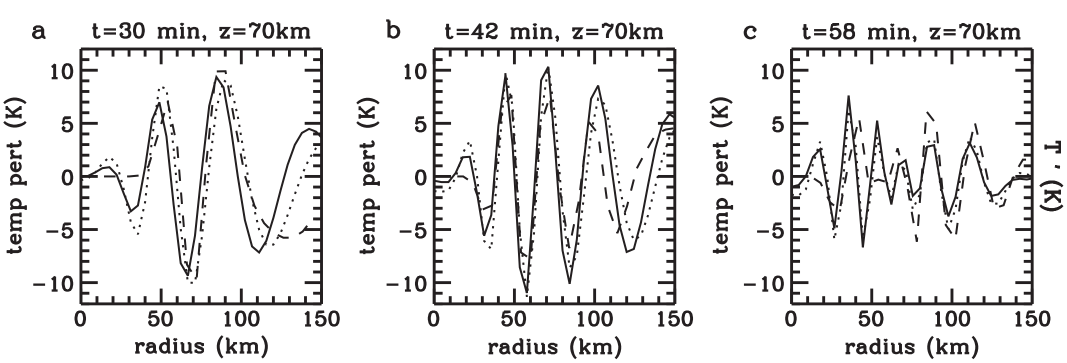

Figure 4. Exact Fourier-Laplace and ray trace solutions at z = 70 km and y = 0 as a function of the radius x of the concentric GW rings. (a) t = 30 min, (b) t = 42 min, and (c) t = 58 min. Solid and dotted lines show the compressible and Boussinesq exact solutions, respectively. Dashed lines show the solutions obtained via ray tracing the compressible solutions from z = 10 km and t = 5 min.

knowledge, this is the first work to calculate the heat/cooling from the dissipation of GWs from a convective plume.

[40] We employ idealized background temperature profiles that are modeled after extreme solar minimum and solar maximum, with exospheric temperatures of 600 and 1200 K, respectively. Figure 5 shows the profiles. Although the actual background wind in the lower atmosphere and thermosphere is quite complicated, we utilize an idealized background wind here in order to understand the basic features of the results. We set $\overline{V}(z) = 0$ and choose a zonal wind that is zero at the ground, becomes westward in the mesosphere, and asymptotes to –70 m/s in the thermosphere:

$$\overline{U}(z) = \frac{1}{2}U_{\text{wind}}\left[1 - \tanh((z - z_d)/\Delta_U)\right] - U_{\text{wind}}, \qquad (68)$$

where $U_{\text{wind}} = -70\ \text{ms}^{-1}$, $z_d = 80$ km, and $\Delta_U = 20$ km. This wind is shown in Figure 5.

[41] We now ray trace the GWs excited by a convective plume from $x = y = 0$, $t = 5$ min and $z = z_{\text{trop}} = 15$ km. Our numerical domain is $x = [-1400, 1400]$ km, $y = [-1400, 1400]$ km, $z = [0, 360]$ km, and $t = [0, 3]$ h. If a GW passes outside this domain, it is eliminated from the spectrum. The cell sizes within this domain (for reconstruction of the GW field in the thermosphere) are 40 km × 40 km × 4 km× 6 min in *x*, *y*, *z*, and *t*, respectively. We reconstruct the GW field using the formalism described in *Vadas and Fritts* [2009].

[42] Upon dissipating, the background fluid is accelerated in the direction of GW propagation. It is also heated by molecular viscosity and can be heat/cooled by the heat flux. The body force and temperature tendencies from GW dissipation are as follows [*Becker*, 2004]:

$$\frac{\partial u}{\partial t} = \ldots - \frac{1}{\overline{\rho}}\frac{\partial}{\partial z}(\overline{\overline{\rho}u'w'}), \qquad (69)$$

$$\frac{\partial v}{\partial t} = \ldots - \frac{1}{\overline{\rho}}\frac{\partial}{\partial z}(\overline{\overline{\rho}v'w'}), \qquad (70)$$

$$C_p\frac{\partial T}{\partial t} = \ldots - \frac{C_p}{\rho}\frac{\partial}{\partial z}\left(\frac{\rho T}{\theta}F_\theta\right) - g\frac{F_\theta}{\theta} + \nu\overline{\left(\frac{\partial}{\partial z}\mathbf{v}'\right)^2}, \qquad (71)$$

$$F_\theta = \overline{\theta' w'}, \qquad (72)$$

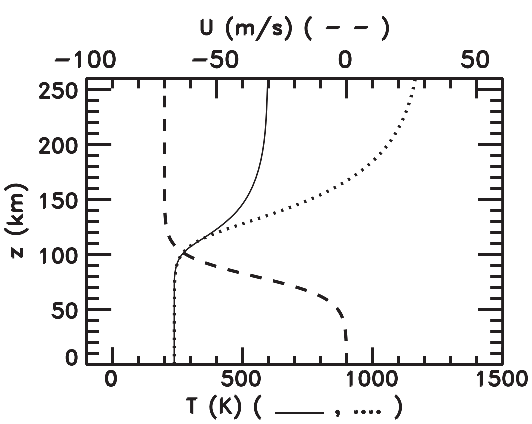

Figure 5. Temperature profiles representing extreme solar minimum (solid line) and solar maximum (dotted line) with exospheric temperatures of 600 K and 1200 K, respectively (lower *x* axis). The zonal wind profile is shown as a dashed line (upper *x* axis).

where F_θ is the vertical flux of potential temperature [*Walterscheid*, 1981] and is loosely referred to here as the "heat flux." The overlines denote averages over one to two wavelengths. Thus, the spatially and temporally varying zonal and meridional components of the body force and heat/cooling (per unit mass) are

$$F_{x,\text{tot}} = -\frac{1}{\overline{\rho}}\frac{\partial\left(\overline{\overline{\rho}u'w'}\right)}{\partial z}, \quad F_{y,\text{tot}} = -\frac{1}{\overline{\rho}}\frac{\partial\left(\overline{\overline{\rho}v'w'}\right)}{\partial z}, \qquad (73)$$

$$J_{\text{tot}} = -\frac{1}{\rho}\frac{\partial}{\partial z}\left(\frac{\rho T}{\theta}F_\theta\right) - \frac{g}{C_p}\frac{F_\theta}{\theta} + \frac{\nu}{C_p}\overline{\left(\frac{\partial}{\partial z}\mathbf{v}'\right)^2}, \qquad (74)$$

respectively. Using the notation from Equations (1)–(3), $F_{x,\text{tot}} = F_x\mathcal{F}$, $F_{y,\text{tot}} = F_y\mathcal{F}$, and $J_{\text{tot}} = J\mathcal{F}$. If the GWs are not dissipating or saturating, 1) $(\overline{\overline{\rho}u'w'})$ and $(\overline{\overline{\rho}v'w'})$ are constant with altitude, so that $F_{x,\text{tot}} = F_{y,\text{tot}} = 0$, and 2) θ' and w' are in quadrature (according to linear theory [*Fritts and Alexander*, 2003]), so that $F_\theta = J_{\text{tot}} = 0$. The first term on the right-hand side of Equation (74) is often referred to as the heat flux convergence due to GWs. This can lead to heating and/or cooling [*Walterscheid*, 1981; *Liu*, 2000]. The second term is the buoyancy production of GW kinetic energy. The third term is the dissipation of GW kinetic energy due to molecular viscosity, which represents the conversion of kinetic to internal energy [*Hines*, 1965]; this term is always positive. Note that Equation (74) is not the quasi-stationary approximation.

[43] We now show the thermospheric body force/heat/coolings created by the dissipation of the primary GWs excited by a deep convective plume with $\mathcal{D}_H = 20$ km, $\chi = 10$ min, and $w_{\text{pl}} = 30$ m/s. Figure 6 shows the results at $t = 75$ min for the exospheric temperature of 600 K. This is the approximate time when the body force/heat/coolings are maximum. Note that the forces are located nearly $\sim \mathcal{H}$ higher than in *Vadas and Fritts* [2006], mainly because of numerical accuracy improvements in the calculation of N_B (i.e., as $N_B{}^2 = (g/\overline{T})(\text{d}\overline{T}/\text{d}z + g/C_p)$ rather than as $N_B{}^2 = (g/\overline{\theta})\,\text{d}\overline{\theta}/\text{d}z$). Although the results using the Boussinesq and compressible GW spectra are similar, the force/heat/cooling amplitudes using the Boussinesq spectra tend to be ∼10–40% larger. This is expected, since the Boussinesq GW amplitudes are somewhat larger for those GWs which contribute the most (see section 3). We now focus on the characteristics of the force/heat/coolings. Because the eastward GWs travel against the wind, they propagate to much higher altitudes (before dissipating) than the northward and southward GWs. This causes the eastward body force to be centered at $z \sim 240$ km, while the north/southward body forces are centered at $z \sim 200$ km. On the other hand, the westward GWs dissipate at lower altitudes because they travel with the wind. This causes the westward body force to be centered at $z \sim 190$ km. For the compressible GW spectra, the magnitudes of the eastward forces are 0.1–0.3 m/s^2, the westward forces are 0.05–0.1 m/s^2, and the north/southward forces are 0.1–0.6 m/s^2. The heat/cooling rates are 0.05–0.15 K/s. Note that the meridional forces have larger amplitudes than the zonal body forces. This is because many of the eastward GWs reflect downward in the thermosphere from the westward wind.

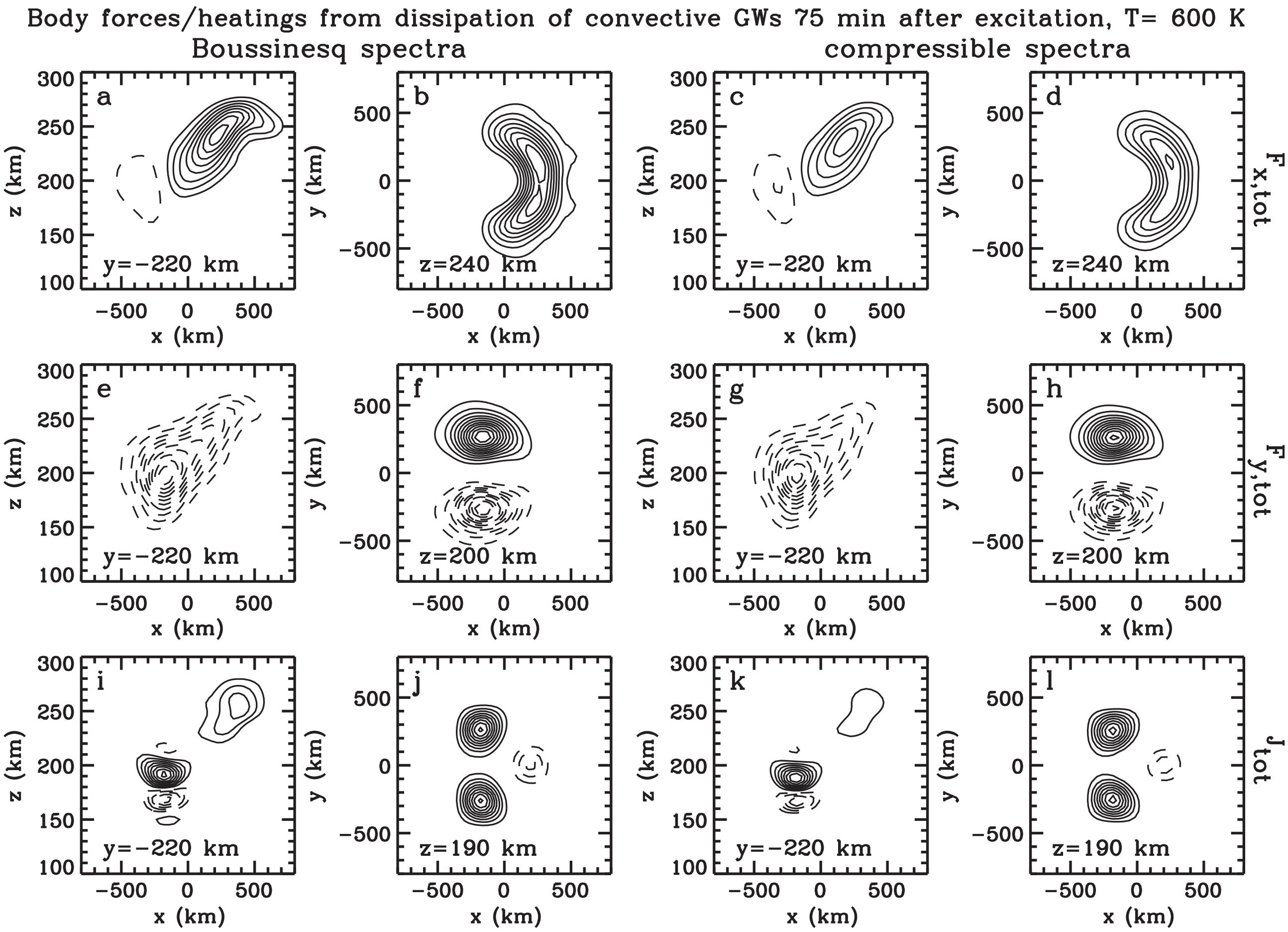

Figure 6. Thermospheric body forces and heat/coolings at t = 75 min created from the dissipation of GWs excited by a deep convective plume. The GWs are ray traced through the thermosphere with exospheric temperature T = 600 K. (a, b, e, f, i, and j) Boussinesq GW spectra. (c, d, g, h, k, and l) Compressible GW spectra. Figures 6a, 6c, 6e, 6g, 6i, and 6k show x-z cross-sections at y = –220 km. Figures 6b, 6d, 6f, 6h, 6j, and 6l show x-y cross-sections at z = 240, 200, and 190 km, as labeled. Rows 1–3 show $F_{x,\mathrm{tot}}$, $F_{y,\mathrm{tot}}$, and J_{tot}, respectively. Solid (dashed) lines show positive (negative) values. Contours in rows 1 and 2 are in intervals of 0.05 m/s^2. Contours in row 3 are in intervals of 0.015 K/s.

[44] Figure 7 shows the results for the exospheric temperature of 1200 K. Again, the results for the Boussinesq and compressible GW spectra are similar, with the amplitudes being somewhat larger for the Boussinesq than the compressible GW spectra. Because $\overline{T}$ is larger than in Figure 6, $\overline{\rho}$ decreases less rapidly, and the kinematic viscosity increases less rapidly. This causes the dissipation of GWs to "spread out" in altitude, thereby leading to smaller force/heat/cooling amplitudes. Additionally, since $\tau_B = 2\pi/N_B$ is larger than during extreme solar minimum, there is more downward reflection in the thermosphere here than in Figure 6, because the convective spectrum has intrinsic periods of 5–20 min (see Figure 3). This causes a substantial loss of eastward-propagating GWs, since they are blue-shifted to higher intrinsic frequencies from the westward wind and reflect downward. For the compressible GW spectra, the magnitudes of the eastward forces are 0.02–0.15 m/s^2, the westward forces are 0.01–0.06 m/s^2, and the north/southward forces are 0.05–0.2 m/s^2. The heat/cooling rates are 0.01–0.06 K/s.

[45] It is important to note that the zonal and meridional body forces are quite deep for both temperature profiles, with full depths of 50–130 km centered at $z \sim 190 - 240$ km. At these altitudes, $\mathcal{H} \sim 20 - 25$ km and $\mathcal{H} \sim 30 - 40$ km for the 600 K and 1200 K thermospheres, respectively. Therefore, these body forces are much deeper than $\mathcal{H}$ in both cases. We show in the next section that the Boussinesq solutions are not adequate for calculating the secondary GW spectra excited by such deep body forces.

[46] We now explore the characteristics of the heat/coolings created by the dissipation of convective GWs in Figures 6 and 7. First, we examine the differences. For the 600 K thermosphere, there is a heating at $z \sim 250$ km where the eastward GWs create a large-amplitude eastward body force. Additionally, there is a smaller-amplitude cooling at $x \sim 200$ km, $y \sim 0$, and z = 190 km, which is below the region where the eastward GWs dissipate and create the eastward body force. For the 1200 K thermosphere, there is little heating at $z \sim 250$ km, and essentially no cooling at $x \sim 200$ km, y = 0, and $z \sim 190$ km.

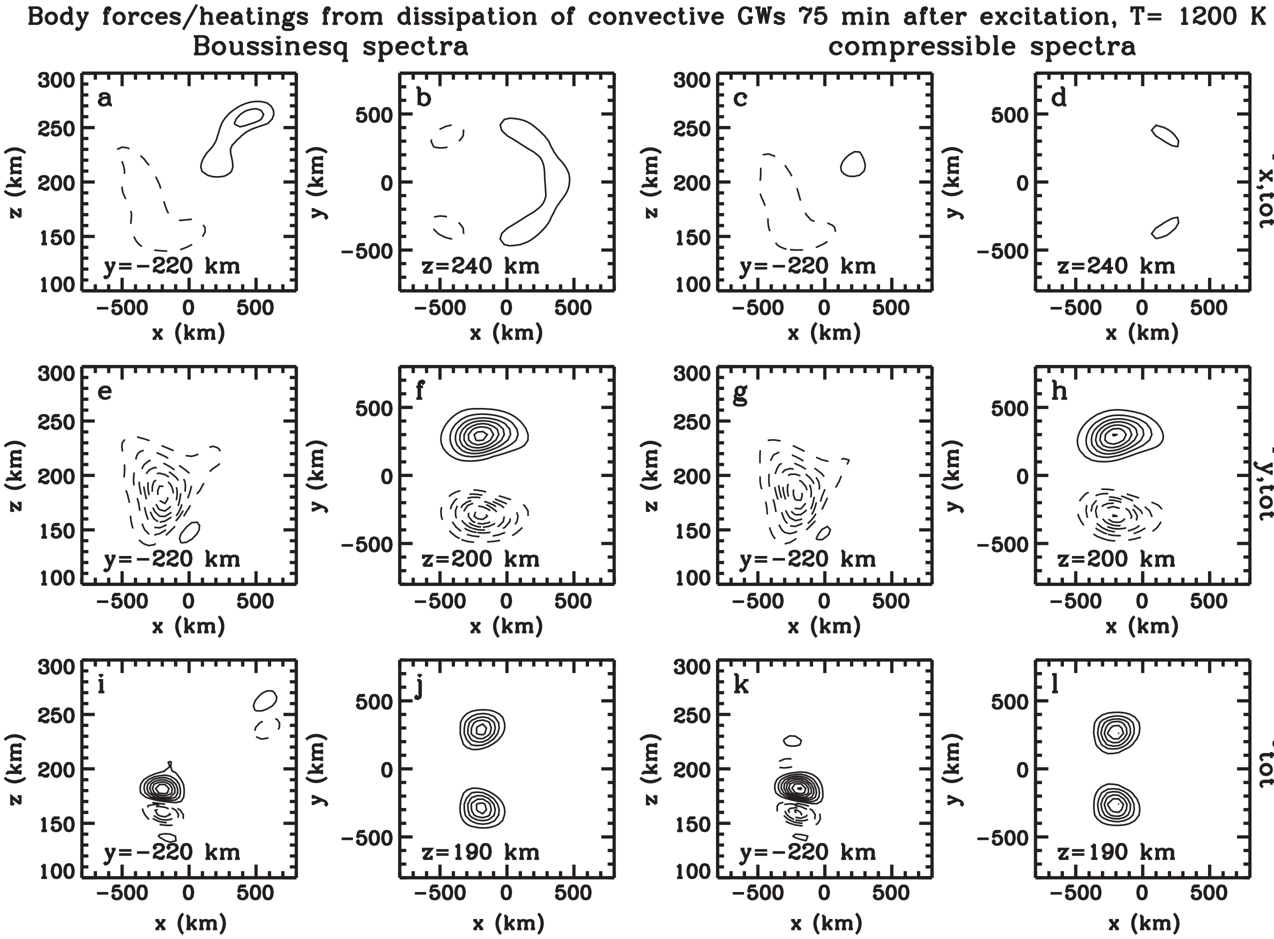

Figure 7. Same as Figure 6 but for the exospheric temperature T = 1200 K. Contours are in intervals of 0.02 m/s^2 in rows 1 and 2, and 0.0075 K/s in row 3.

[47] Next we examine the similarities. Horizontal cuts at z = 190 km show two regions of heating at x = –200 km and $y = \pm 250$ km; these regions coincide with the locations where GWs create large-amplitude north and southward body forces. The vertical cuts at y = –220 km show that these heatings are part of dipoles, with heatings (at $z \sim$180–210 km) above coolings (at $z \sim$160–170 km). There are also small-amplitude coolings (heatings) above (below) the dipoles at $z \sim$220 km ($z \sim$150 km). Note that the depths of the dipoles is $\mathcal{D}_z \sim$40–50 km $> \mathcal{H}$. We show in the next section that the compressible solutions are necessary for calculating the secondary GW spectra excited by these heat/coolings.

[48] Figure 8 shows the contributions to the heat/cooling at t = 75 min from the first, second, and third terms on the right-hand side of Equation (74), respectively. Here, we ray trace the compressible GW spectrum through the 600 K thermosphere. The heat flux convergence term clearly dominates and creates the heat/cool dipole at $z \sim$150–210 km. However, the heating due to molecular viscosity accounts for nearly all of the heating which occurs at $z \sim$ 240 km from the dissipation of northeast, east, and southeastward GWs. Note that the buoyancy production of GW kinetic energy (second term) is negligible.

[49] Figure 9 shows the heat flux, F_θ, for the same time and locations as in Figure 8. In the region where heating occurs ($x \sim y \sim$ –200 km and $z \sim$ 180 km), the heat flux is positive. This suggests that w' and θ' are less than 90° out of phase there. In fact, *Vadas and Nicolls* [2012] showed that the phase shift between w' and T' decreases (< 90°) as a GW within a wave packet dissipates. This equals the phase shift between w' and θ' for medium-scale GWs with $|\lambda_z| < 2\pi\mathcal{H}$, since $\theta' \sim T'$ when the pressure perturbations are small. However, we must be careful not to extrapolate monochromatic GW results to GW spectral results, since *Walterscheid* [1981] noted that a spectrum of GWs may behave differently than a monochromatic wave because of constructive/destructive wave interference.

[50] Finally, we note that *Liu* [2000] calculated the heat/cooling caused by the breaking of a monochromatic GW using saturation theory. They also found that a dipole was created but with cooling above the heating. This result depended sensitively on the turbulent Prandtl number and the localization of the breaking region.

5. Secondary GWs Excited by Forces and Heatings in the Thermosphere

[51] In this section, we calculate the secondary GWs excited by idealized body forces and heatings in the thermosphere. In order to understand the basic differences between the compressible and Boussinesq GW spectra, we

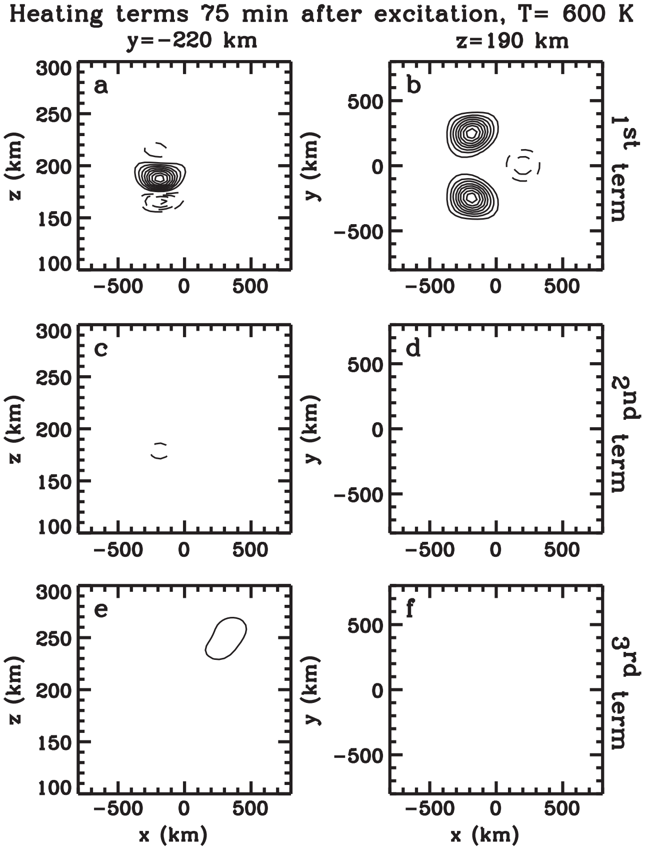

Figure 8. Heat/cooling contributions from Figure 6. Rows 1–3 show the first, second, and third terms on the right-hand side of Equation (74), respectively. (a, c, and e) x-z cross-sections at y = –220 km. (b, d, and f) x-y cross-sections at z = 190 km. Solid (dashed) lines show positive (negative) values. Contours are in intervals of 0.015 K/s.

calculate the GW spectra for simple force/heatings. The spatial scales for these force/heatings include those which occur from the dissipation of GWs from a deep convective plume (see section 4).

[52] First, we argue that the body force/heat/coolings created by convective plumes excite only medium and high-frequency GWs. From Figures 6 and 7, the ratio of the horizontal width to vertical depth is ∼3–5 for the forces and ∼5–10 for the heat/coolings. If the force/heat/cooling duration is not too long, the peak periods of the excited GWs is ∼ τ_B times this ratio (VF01). Since τ_B ∼7–10 min at z ∼180–200 km and τ_B ∼9–12 min at z ∼220–250 km, we estimate GW peak periods of τ_{Ir} ∼20–60 min for the forces and τ_{Ir} ∼35–100 min for the heat/coolings. The force durations from deep convection are $\chi < 15$ min [*Vadas and Crowley*, 2010]; this is also likely true for the heat/coolings. Since $\chi < \tau_{Ir}$, we estimate GW peak periods of τ_{Ir} ∼20–100 min. Therefore, the Coriolis force is not important, so we set $f = 0$. In this limit, the compressible solutions from forces and heat/coolings simplify considerably.

5.1. Secondary GWs from Horizontal Body Forces

[53] The postforcing ($t \geq \chi$) compressible zonal and vertical velocity perturbations from a zonal body force F_x with $f = 0$ (using Equations (45), (47), (13), and (14)) are

$$\left(\widetilde{e^{-z/2\mathcal{H}}u'}\right) = \frac{l^2}{k_H^2}\left(\widetilde{e^{-z/2\mathcal{H}}F_x}\right) + \frac{k^2}{N_B^2 k_H^2}\left[\frac{1}{1-\omega_1^2/\omega_2^2}\right]\left(\widetilde{e^{-z/2\mathcal{H}}F_x}\right) \left\{\left(N_B^2-\omega_1^2\right)\frac{\hat{a}^2\mathcal{S}(\omega_1)}{\chi\omega_1(\hat{a}^2-\omega_1^2)} - \frac{\omega_1^2}{\omega_2^2}\left(N_B^2-\omega_2^2\right) \times\frac{\hat{a}^2\mathcal{S}(\omega_2)}{\chi\omega_2(\hat{a}^2-\omega_2^2)}\right\}, \tag{75}$$

$$\left(\widetilde{e^{-z/2\mathcal{H}}w'}\right) = \frac{km\omega_1^2}{k_H^2 N_B^2}\left[\frac{1+i\left(\frac{2-\gamma}{2\gamma\mathcal{H}m}\right)}{1-\omega_1^2/\omega_2^2}\right]\left(\widetilde{e^{-z/2\mathcal{H}}F_x}\right) \left\{-\frac{\hat{a}^2\mathcal{S}(\omega_1)}{\chi\omega_1\left(\hat{a}^2-\omega_1^2\right)} + \frac{\hat{a}^2\mathcal{S}(\omega_2)}{\chi\omega_2\left(\hat{a}^2-\omega_2^2\right)}\right\}. \tag{76}$$

The zonal (vertical) velocity perturbations contain mean, GW, and AW (GW and AW) components. From VF01, the postforcing ($t \geq \chi$) Boussinesq zonal and vertical velocity perturbations that arise from a zonal body force with $f = 0$ are as follows:

$$\widetilde{u'} = \frac{l^2}{k_H^2}\widetilde{F_x} + \left\{\frac{k^2}{k_H^2}\left(1-\frac{\omega_1^2}{N_B^2}\right)\frac{\hat{a}^2}{\chi\omega_1\left(\hat{a}^2-\omega_1^2\right)}\mathcal{S}(\omega_1)\right\}\widetilde{F_x}, \tag{77}$$

$$\widetilde{w'} = -\frac{km}{k_H^2}\frac{\omega_1^2}{N_B^2}\frac{\hat{a}^2}{\chi\omega_1\left(\hat{a}^2-\omega_1^2\right)}\widetilde{F_x}\mathcal{S}(\omega_1). \tag{78}$$

Results similar to Equations (75)–(78) are obtained for a meridional body force F_y (i.e., replace $k \to l$ and $l \to k$, $F_x \to F_y$, and $u' \to v'$). As before, it is easy to show that the compressible mean and GW solutions reduce to the Boussinesq solutions for $\mathcal{H} \to \infty$ and $c_s^2 \to \infty$, since $\omega_1^2/\omega_2^2 \simeq b/a^2 \propto c_s^{-2}$.

[54] There are several differences between the compressible and Boussinesq GW solutions. First, the zonal body force is multiplied by $\exp(-z/2\mathcal{H})$ before applying the Fourier transform. Therefore, if the depth of the body force is greater than $\mathcal{H}$, compressible effects are expected to be important. Second, the compressible GW solutions include the extra terms in the square brackets in Equations (75)–(76). The numerator of the [ ] term in Equation (76)

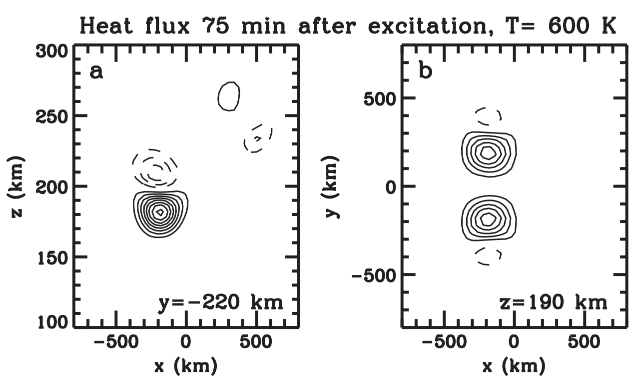

Figure 9. Heat flux, F_θ, for the same GWs as in Figure 8. (a) The x-z cross-section at y = –220 km and (b) the x-y cross-section at z = 190 km. Contours are in intervals of 1×10^5 K m/s. Solid (dashed) lines show positive (negative) values.

equals one if $\mathcal{H}|m| \gg 1$ (i.e., if $|\lambda_z| \ll 2\pi\mathcal{H}$). The denominators of the [ ] terms in Equations (75) and (76) equal one if $\omega_1^2/\omega_2^2 \ll 1$; from Equations (31) and (32), this is satisfied if $4b/a^2 \ll 1$ or $2N_B/c_s \ll (\mathbf{k}^2 + 1/4\mathcal{H}^2)/k_H$. Setting $\omega_1^2 = {k_H}^2 N_B^2/\left(\mathbf{k}^2 + 1/4\mathcal{H}^2\right)$, this condition becomes $c_H \ll c_s/2$, where $c_H = \omega_1/k_H$ is the horizontal phase speed. Therefore, the Boussinesq solutions are only expected to be adequate if $|\lambda_z| \ll 2\pi\mathcal{H}$ or $c_H \ll c_s/2$.

[55] We now apply these solutions to the zonal and meridional body forces created in the thermosphere from the dissipation of GWs from a deep convective plume. From Figures (6) and (7), the vertical depths of the largest-amplitude forces are ∼70–120 km. Since $\mathcal{H}$ ∼20–45 km at z ∼190–250 km, the forces are therefore much deeper than $\mathcal{H}$. We calculate the GWs excited by a simple, Gaussian, meridional body force:

$$F_y = v_0 \exp\left(-\left[\frac{(x-x_0)^2}{2\sigma_x^2} + \frac{(y-y_0)^2}{2\sigma_y^2} + \frac{(z-z_0)^2}{2\sigma_z^2}\right]\right). \tag{79}$$

We choose $x_0 = y_0 = 0$, $z_0 = 200$ km, a full width of $\mathcal{D}_H = 4.5\sigma_x = 4.5\sigma_y = 300$ km, a duration of $\chi = 15$ min, and full depths of $\mathcal{D}_z = 4.5\sigma_z = 10$ km, 50, and 100 km. We utilize the extreme solar minimum temperature profile; at $z = 200$ km, $\overline{T} = 545$ K, $\mathcal{H} = 21$ km, $c_s = 545$ m/s, $N_B = 0.012$ rad/s, $\gamma = 1.5$, and $X_{MW} = 23$. We also set $f = 0$.

[56] Figures 10a, 10b, 10d, 10e, 10g, and 10h show the Boussinesq and compressible 2-D spectra of the vertical flux of meridional momentum for GWs with $k = 0$. The spectra for the deeper forces peak at $|\lambda_z| \sim 2\mathcal{D}_z$. The spectra contain GWs with λ_H ∼200–1200 km and τ_{Ir} ∼20–300 min for the shallow force ($\mathcal{D}_z = 10$ km), and λ_H ∼200–5000 km and τ_{Ir} ∼15–180 min for the deep force ($\mathcal{D}_z = 100$ km). Figures 10c, 10f, and 10i show the fractional differences between the solutions. The Boussinesq and compressible spectra are nearly identical for the shallow force (since $\mathcal{D}_z < \mathcal{H}$). However, for $\mathcal{D}_z = 50$ and 100 km ($> \mathcal{H}$), the Boussinesq and compressible spectra are quite different; they differ by ≥50% for $|\lambda_z| > 200$ km, and ≥100% for $\lambda_H > 2000$ km and $|\lambda_z| > 300$ km. In general, these solutions differ substantially for GWs with $|\lambda_z| > 2\pi\mathcal{H}$ for forces deeper than $\mathcal{H}$.

[57] We now discuss the applicability of Figure 10 for the thermospheric body forces resulting from the dissipation of GWs excited by a deep convective plume. The force with $\mathcal{D}_z = 10$ km is too shallow to represent a realistic force, while the forces with $\mathcal{D}_z = 50$ and 100 km represent realistic depths (see Figures 6 and 7). Because $\mathcal{D}_z > \mathcal{H}$, the Boussinesq solutions therefore cannot adequately represent the excited secondary GWs; instead, the compressible solutions must be utilized. From Figures 10d–10i, we estimate the secondary GWs from a single plume to have λ_H ∼200–4000 km, $|\lambda_z|$ ∼50–1000 km, intrinsic periods of τ_{Ir} ∼15–180 min, and intrinsic horizontal phase speeds of c_{IH} ∼100–500 m/s. These are similar to the GWs identified by *Vadas and Crowley* [2010].

[58] Figure 10 shows the GW parameters for $z_{\text{diss}} = 200$ and 250 km. For the force with $\mathcal{D}_z = 50$ km, more than 1/2 of the secondary GWs propagate above $z = 200$ km prior to dissipating; the other 1/2 dissipate in the force region. Additionally, many secondary GWs can propagate above $z = 250$ km prior to dissipating. For the force with $\mathcal{D}_z = 100$ km, virtually all of the secondary GWs propagate out of the force region. Additionally, ∼ 1/2 of the secondary GWs propagate above $z = 250$ km prior to dissipating.

5.2. Secondary GWs Excited by Heat/Coolings in the Thermosphere

[59] The postforcing ($t \geq \chi$) compressible zonal and vertical velocity perturbations from a heating with $f = 0$ (using Equations (45), (47), (13), and (14)) are

$$\left(\widetilde{e^{-z/2\mathcal{H}}u'}\right) = \frac{km\omega_1^2}{k_H^2 N_B^2}\left[\frac{1}{1-\omega_1^2/\omega_2^2}\right]\left(\frac{\mathrm{r}}{\gamma\mathcal{H}}\widetilde{e^{-z/2\mathcal{H}}J}\right)\frac{\hat{a}^2}{\chi}$$
$$\left\{\frac{\left[1+i\left(\frac{\omega_1^2}{gm}-\frac{1}{2m\mathcal{H}}\right)\right]\mathcal{C}(\omega_1)}{\omega_1^2\left(\hat{a}^2-\omega_1^2\right)} - \frac{\left[1+i\left(\frac{\omega_2^2}{gm}-\frac{1}{2m\mathcal{H}}\right)\right]\mathcal{C}(\omega_2)}{\omega_2^2\left(\hat{a}^2-\omega_2^2\right)}\right\}, \tag{80}$$

$$\left(\widetilde{e^{-z/2\mathcal{H}}w'}\right) = -\frac{m^2\omega_1^2}{k_H^2 N_B^2}\left[\frac{1+i\left(\frac{2-\gamma}{2\gamma\mathcal{H}m}\right)}{1-\omega_1^2/\omega_2^2}\right]\left(\frac{\mathrm{r}}{\gamma\mathcal{H}}\widetilde{e^{-z/2\mathcal{H}}J}\right)\frac{\hat{a}^2}{\chi}$$
$$\left\{\frac{\left[1+i\left(\frac{\omega_1^2}{gm}-\frac{1}{2m\mathcal{H}}\right)\right]\mathcal{C}(\omega_1)}{\left(N_B^2-\omega_1^2\right)\left(\hat{a}^2-\omega_1^2\right)} - \frac{\left[1+i\left(\frac{\omega_2^2}{gm}-\frac{1}{2m\mathcal{H}}\right)\right]\mathcal{C}(\omega_2)}{\left(N_B^2-\omega_2^2\right)\left(\hat{a}^2-\omega_2^2\right)}\right\}. \tag{81}$$

As before, the heat function is multiplied by $\exp(-z/2\mathcal{H})$ before taking the Fourier transform. Because the numerators of the GW terms in square brackets are proportional to $1/m\mathcal{H}$, compressible effects are expected to be important for $|\lambda_z| > 2\pi\mathcal{H}$. We compare these solutions to the Boussinesq solutions. From VF01, the postforcing ($t \geq \chi$) Boussinesq zonal and vertical velocity perturbations from a heating with $f = 0$ are as follows:

$$\widetilde{u'} = \frac{km\omega_1}{k_H^2 N_B^2}\frac{\hat{a}^2}{\chi\omega_1\left(\hat{a}^2-\omega_1^2\right)}\widetilde{J_B}\mathcal{C}\left(\omega_1\right), \tag{82}$$

$$\widetilde{w'} = -\frac{\omega_1}{N_B^2}\frac{\hat{a}^2}{\chi\omega_1\left(\hat{a}^2-\omega_1^2\right)}\widetilde{J_B}\mathcal{C}\left(\omega_1\right). \tag{83}$$

Using Equation (7) and $m^2\omega_1^2 = k_H^2(N_B^2 - \omega_1^2)$ in the Boussinesq limit, it is easy to verify that the compressible solutions reduce to the Boussinesq solutions for $\mathcal{H} \to \infty$ and $c_s^2 \to \infty$.

[60] We calculate the GWs excited by a simple Gaussian heating:

$$J = J_0 \exp\left(-\left[\frac{(x-x_0)^2}{2\sigma_x^2} + \frac{(y-y_0)^2}{2\sigma_y^2} + \frac{(z-z_0)^2}{2\sigma_z^2}\right]\right). \tag{84}$$

We choose a full width of $\mathcal{D}_H = 300$ km, a duration of $\chi = 15$ min, and full depths of $\mathcal{D}_z = 10$ km and 30 km. All other parameters are the same as in Figure 10.

[61] Figures 11a, 11b, 11d, and 11e show the Boussinesq and compressible 2-D spectra of the vertical flux of zonal momentum for the GWs with $l = 0$. The spectra peak at $|\lambda_z| \sim (2-4)\mathcal{D}_z$ and $\lambda_H \sim (1.5-2)\mathcal{D}_H$. The GWs have τ_{Ir} ∼20–200 min, with λ_H ∼200–1600 km for the shallow force ($\mathcal{D}_z = 10$ km) and λ_H ∼200–3000 km for the deeper

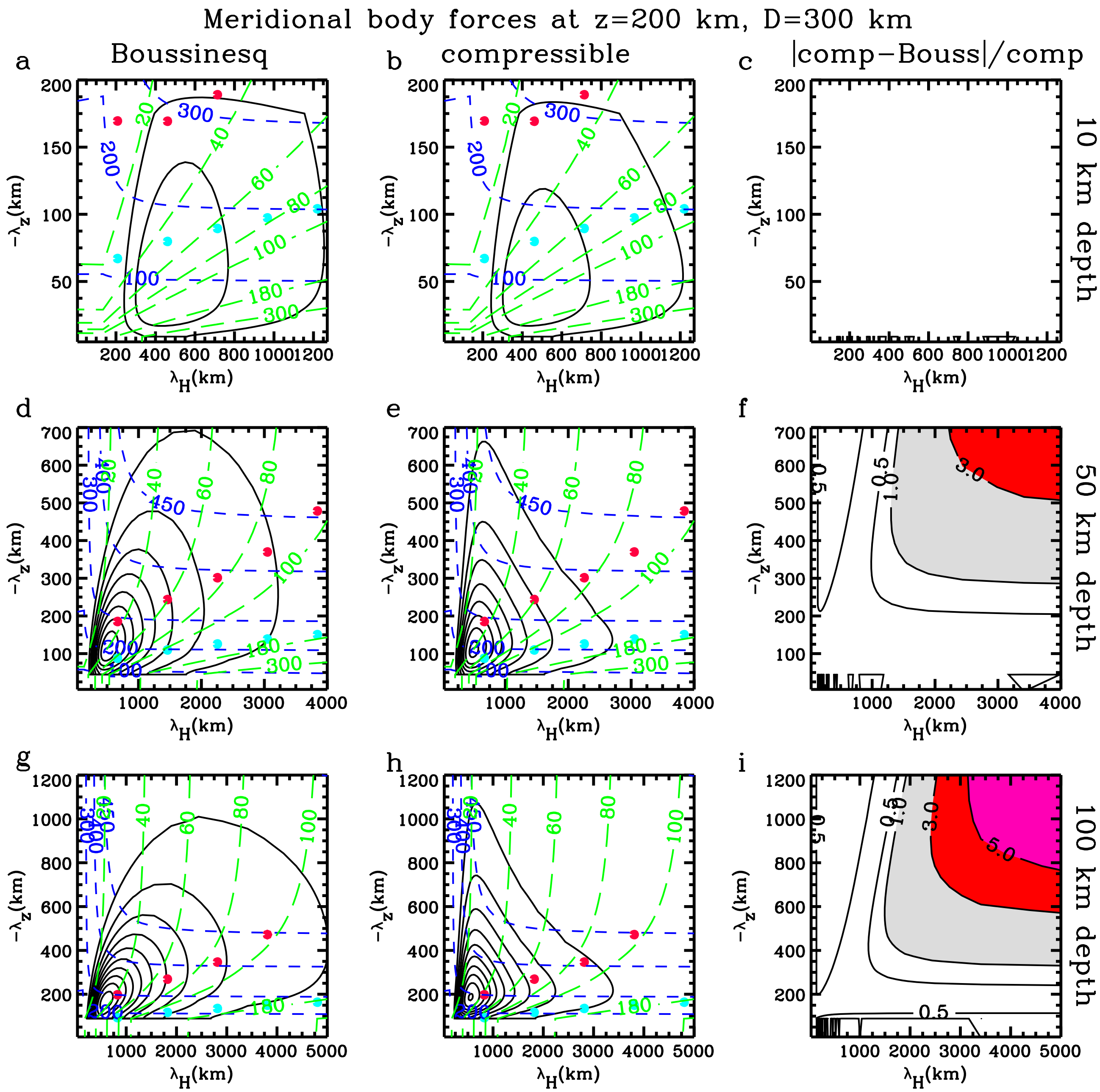

Figure 10. Vertical flux of meridional momentum for the GWs excited by a Gaussian meridional body force at z = 200 km with a full width of $\mathcal{D}_H$ = 300 km. Contours show 10% intervals of an arbitrary value. Row 1: (a) Boussinesq (solid) and (b) compressible (solid) solutions for $\mathcal{D}_z$ = 10 km. (c) |Compressible–Boussinesq|/compressible solutions from Figures 10a and 10b (solid). The gray, red, and pink shaded contours show the values 1, 3, and 5, respectively. Rows 2 and 3: Same as row 1 but for $\mathcal{D}_z$ = 50 km and $\mathcal{D}_z$ = 100 km, respectively. The turquoise and red dots show z_{diss} = 200 km and 250 km, respectively. Blue short-dashed lines indicate c_{IH} (in m/s), and green long-dashed lines show τ_{Ir} (in min).

force ($\mathcal{D}_z$ = 30 km). Figures 11c, 11f, and 11i show the fractional differences between the solutions. Because $\mathcal{D}_z < \mathcal{H}$, the Boussinesq and compressible spectra are nearly identical for the shallow heating. However, for the deeper heating ($\mathcal{D}_z > \mathcal{H}$), the Boussinesq and compressible spectra differ by $\geq$100% for λ_H > 1000 km and $|\lambda_z|$ > 300 km. Thus, the solutions differ substantially for GWs with $|\lambda_z| > 2\pi\mathcal{H}$ for heatings deeper than $\mathcal{H}$.

[62] We now discuss the applicability of the examples shown in Figure 11 for the heat/coolings created by the dissipation of GWs excited by a deep convective plume. The heating with $\mathcal{D}_z$ = 10 km is too shallow to represent a realistic heating, while the heating with $\mathcal{D}_z$ = 30 km represents a realistic depth (see Figures 6 and 7). Additionally, many of the heat/coolings occur as deeper (∼50–60 km) dipoles. Because $\mathcal{D}_z > \mathcal{H}$, it is necessary to model the excitation

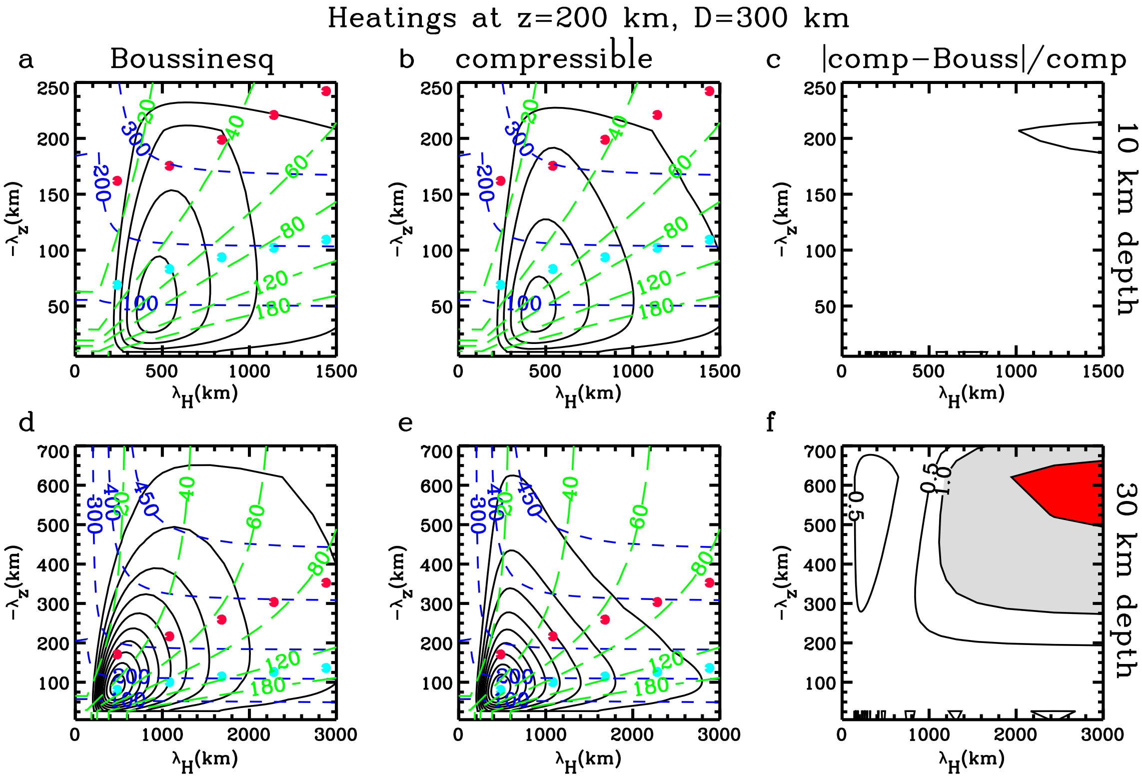

Figure 11. Vertical flux of zonal momentum for the GWs excited by a Gaussian heating at z = 200 km with a full width of $\mathcal{D}_H$ = 300 km. Contours show 10% intervals of an arbitrary value. Row 1: (a) Boussinesq (solid) and (b) compressible (solid) solutions for $\mathcal{D}_z$ = 10 km. (c) |Compressible–Boussinesq|/compressible solutions from Figures 11a and 11b (solid). The gray and red shaded contours show the values 1 and 3, respectively. Row 2: Same as row 1 but for $\mathcal{D}_z$ = 30 km. The turquoise and red dots show z_{diss} = 200 km and 250 km, respectively. Blue short-dashed lines indicate c_{IH} (in m/s), and green long-dashed lines show τ_{Ir} (in min).

of secondary GWs from the heat/coolings using the compressible solutions. From Figures 11d and 11e, we estimate the secondary GWs to have $\lambda_H \sim$200–3000 km, $|\lambda_z| \sim$20–700 km, intrinsic periods of $\tau_{Ir} \sim$10–200 min, and intrinsic horizontal phase speeds of $c_{IH} \sim$100–500 m/s. Note that $\sim$ 1/2 of the secondary GWs propagate out of the force region prior to dissipating, and many propagate to $z > 250$ km prior to dissipating.

6. Conclusions

[63] In this paper, we derived the *f*-plane, compressible, linear solutions to local, interval body forcings and heat/coolings in an isothermal, unsheared, and nondissipative atmosphere. These force/heat/coolings oscillate at the frequency $\hat{\alpha}$ and turn on and off smoothly over a finite interval in time. The solutions include a mean response, GWs, and AWs. We found that the compressible solutions are important for correctly calculating the amplitudes of the excited GWs which have $|\lambda_z| >$ (1 to 2) $\times\, \pi\mathcal{H}$ if the force/heat/cooling depth is greater than $\mathcal{H}$.

[64] We applied these solutions to the excitation of primary GWs in the lower stratosphere from a single convective plume. Such a plume has been modeled as a vertical body force in previous work [*Vadas and Fritts*, 2009; *Vadas et al.*, 2009b, 2012]. We found that the compressible solutions (derived in this paper) are only needed to describe those deep primary GWs with $|\lambda_z| >$ (1 to 2) $\times\, \pi\mathcal{H}$. However, because these are the GWs which can penetrate deeply into the thermosphere, these compressible solutions are therefore needed for studies involving the impact of GWs from deep convection on the thermosphere.

[65] We ray traced (with phases) the Boussinesq and compressible GW spectra from the plumes into the thermosphere using idealized extreme solar minimum and solar maximum temperature profiles and an idealized 0 to –70 m/s westward wind. Kinematic viscosity and thermal diffusivity damped the GWs in the thermosphere. We calculated the body forces and heat/coolings created by the dissipation of these primary GWs. We found that the body force amplitudes using the compressible GW spectra were 10–40% smaller than those using the Boussinesq GW spectra. In both cases, zonal and meridional body forces were created in the thermosphere; the zonal forces were located at $z \sim$240–250 km east of the plume, and the meridional forces were located at $z \sim$200 km north and south of the plume. Because of the large westward wind and high frequencies within the initial GW spectrum, many of the eastward GWs had their intrinsic frequencies blue-shifted to the buoyancy

frequency, causing them to reflect downward. This caused the amplitude of the eastward body force to be smaller than the amplitudes of the meridional body forces. All body forces were located a few hundred kilometers horizontally from the plume and were maximum $\sim$75 min after convective overshoot. For a 20 km diameter plume with an updraft velocity of 30 m/s, the maximum amplitudes for the horizontal body forces were 0.6 m/s^2 and 0.2 m/s^2 for the 600 K and 1200 K thermospheres, respectively. Thus, the body force amplitudes were $\sim$3 times larger during extreme solar minimum than during solar maximum. This occurred because the GW dissipation altitudes are more "spread out" during solar maximum, since the viscosity increases less rapidly in altitude.

[66] We also calculated the heat/cooling which occurred in the thermosphere due to the dissipation of these primary GWs. We found that a high-altitude heating (z $\sim$250–260 km) occurs where the eastward GWs dissipate. This heating was caused by molecular viscosity. Where the northward/southward GWs dissipated, however, the heat flux convergence created dipoles, with heating above cooling. Here, the heating was centered at z $\sim$190–200 km, and the cooling was centered at z $\sim$160–170 km. The maximum amplitudes for the heat/coolings were 0.15 K/s and 0.06 K/s for the 600 K and 1200 K thermospheres, respectively. Thus, the amplitudes were $\sim$2–3 times larger during extreme solar minimum than during solar maximum for the same reason as for the body forces. Note that the heat/coolings were displaced a few hundred kilometers horizontally from the plume and were maximum $\sim$75 min after convective overshoot.

[67] We then calculated the GWs excited by Gaussian horizontal body forces and heatings in the thermosphere. We found that if the depth of the force/heating, $\mathcal{D}_z$, was less than $\mathcal{H}$, the Boussinesq solutions were adequate for determining the excited GW spectrum. However, if $\mathcal{D}_z > \mathcal{H}$, the compressible solutions were necessary for determining the excited GW spectrum.

[68] We applied these solutions to the secondary GWs from a deep convective plume. Because $\mathcal{D}_z > \mathcal{H}$ for the force/heat/coolings created from the dissipation of GWs from a deep convective plume, we concluded that the compressible solutions are necessary for calculating the excited secondary GWs. For a single plume, we estimated the secondary GWs to have λ_H $\sim$200–4000 km, $|\lambda_z|$ $\sim$20–1100 km, τ_{Ir} $\sim$10–200 min, and c_{IH} $\sim$100–500 m/s. However, constructive and destructive interference of GWs from multiple plumes create forces with smaller horizontal extents, thereby exciting smaller-λ_H GWs [*Vadas and Crowley*, 2010]. Future work will calculate the secondary GWs excited by thermospheric body force/heat/coolings generated from multiple plumes.

Appendix A: Total Energy Equation

[69] In this appendix, we derive the equation for the total energy. For a perfect gas, the internal energy per unit volume is ρe, where $e = C_v T$ is the internal energy per unit mass [*Kundu*, 1990]. Using Equations (2) and (3),

$$\frac{\mathrm{D}(\rho e)}{\mathrm{D}t} = -\gamma\rho e\nabla.\mathbf{v} + C_v\rho J\mathcal{F}. \quad \text{(A1)}$$

From Equations (1) and (2),

$$\frac{\mathrm{D}\left(\rho\frac{1}{2}\mathbf{v}.\mathbf{v} + \rho g z\right)}{\mathrm{D}t} = -(\mathbf{v}.\nabla)p - \rho\left(\frac{1}{2}\mathbf{v}.\mathbf{v} + gz\right)\nabla.\mathbf{v} + \rho\mathbf{v}.\mathbf{F}\mathcal{F}, \quad \text{(A2)}$$

where $\mathbf{g} = -g\hat{k}$, so that $\mathbf{v}.\mathbf{g} = -\mathbf{v}.\nabla(gz) = -\mathrm{D}(gz)/\mathrm{D}t$. Additionally, $\mathbf{v}.(\mathbf{\Omega}\times\mathbf{v}) = 0$, since $\mathbf{\Omega}\times\mathbf{v}$ is perpendicular to $\mathbf{v}$. The quantity "$\rho\frac{1}{2}\mathbf{v}.\mathbf{v} + \rho g z$" is the kinetic plus potential energy per unit volume. We define the total energy per volume to be

$$\mathcal{E} = \rho\frac{1}{2}\mathbf{v}.\mathbf{v} + \rho g z + \rho e. \quad \text{(A3)}$$

Equation (A3) differs from Equation (3.25) in VF01 because that formula contains the wave energy density instead (e.g., Equation. (2.6) of *Bretherton* [1969]). Adding Equations (A1) and (A2) and using $\mathrm{D}\mathcal{E}/\mathrm{D}t = \partial\mathcal{E}/\partial t + \nabla.(\mathcal{E}\mathbf{v}) - \mathcal{E}\nabla.\mathbf{v}$, we obtain the total energy equation:

$$\frac{\partial\mathcal{E}}{\partial t} + \nabla.(\mathcal{E}\mathbf{v}) = -\nabla.(p\mathbf{v}) + \rho(\mathbf{v}.\mathbf{F} + C_v J)\mathcal{F}. \quad \text{(A4)}$$

Using Gauss' Theorem, $\int_V \nabla.(\mathcal{E}\mathbf{v})dV = \int_A \mathcal{E}(\mathbf{v}.d\mathbf{A})$, we integrate Equation (A3) over a large-enough volume V to contain the forcings/heat/coolings and dynamical response:

$$\frac{\partial}{\partial t}\int_V \mathcal{E}\mathrm{d}V + \int_A \mathcal{E}\mathbf{v}.\mathrm{d}\mathbf{A} = -\int_A p\mathbf{v}.\mathrm{d}\mathbf{A} + \int_V \mathcal{F}\rho(\mathbf{v}.\mathbf{F} + C_v J)\mathrm{d}V. \quad \text{(A5)}$$

Here, A is the surface which encloses V, and $\mathbf{A}$ is A times the unit vector perpendicular to this surface. Because $\mathbf{v} = 0$ on this surface, $\mathbf{v}.d\mathbf{A} = 0$. The change in time of the total energy within V is due only to the forcings and heat/coolings:

$$\frac{\partial}{\partial t}\int_V \mathcal{E}\mathrm{d}V = \int_V \mathcal{F}\rho(\mathbf{v}.\mathbf{F} + C_v J)\mathrm{d}V. \quad \text{(A6)}$$

The first term on the right-hand side of Equation (A6), $\mathcal{F}\rho\mathbf{v}.\mathbf{F}$, expresses the work done on the fluid by the external force $\mathbf{F}$ per unit volume. The second term, $\mathcal{F}\rho C_v J$, expresses the total energy added to the fluid by the heating per unit volume. This latter term differs from Eq. (3.24) of VF01 because only the wave energy was considered in that formula. In that case, the contribution from the heat/cooling to the wave energy was $(g/N_B^2)(\theta'/\overline{\theta})J_B = (\mathrm{g}r/\gamma\mathcal{H}N_B^2)(\theta'/\overline{\theta})J = C_v(\theta'/\overline{\theta})J$, where we have used Equations (7), (21), and (27). For a linear solution ($|\theta'/\overline{\theta}| \ll 1$), the heat/cooling contributes more to the total energy than to the wave energy.

Appendix B: Compressible, *f*-plane, Nondissipative Polarization Relations

[70] In this appendix, we derive the compressible, *f*-plane, nondissipative polarization relations for GWs and AWs. We assume GW and AW plane wave solutions of the form

$$\xi(x, y, z, t) = \mathrm{e}^{i(\omega_r t - kx - ly - mz)}\widetilde{\xi}(k, l, m). \quad \text{(B1)}$$

This follows the same form as Equation (15). We define the "hatted" quantities as follows:

$$\begin{aligned}
\hat{u} &= \left(\widetilde{\mathrm{e}^{-z/2\mathcal{H}}u'}\right) = \widetilde{\xi}, \qquad \hat{v} = \left(\widetilde{\mathrm{e}^{-z/2\mathcal{H}}v'}\right) = \widetilde{\sigma},\\
\hat{w} &= \left(\widetilde{\mathrm{e}^{-z/2\mathcal{H}}w'}\right) = \widetilde{\eta}, \qquad \hat{\rho} = \left(\widetilde{\mathrm{e}^{-z/2\mathcal{H}}\rho'/\overline{\rho}}\right) = \widetilde{\phi},\\
\hat{p} &= \left(\widetilde{\mathrm{e}^{-z/2\mathcal{H}}p'/\overline{p}}\right) = \widetilde{\psi}, \qquad \hat{T} = \left(\widetilde{\mathrm{e}^{-z/2\mathcal{H}}T'/\overline{T}}\right) = \widetilde{\zeta}, \quad \text{(B2)}
\end{aligned}$$

where the widetilde " $\sim$ " encompasses all factors within each parenthesis. Using Equations (16)–(20), (13), and (B1), we obtain the exact, compressible, nondissipative *f*-plane polarization relations for both GWs and AWs:

$$\hat{u} = \frac{ik\omega_{Ir} + fl}{il\omega_{Ir} - fk}\hat{v}, \tag{B3}$$

$$\hat{p} = \frac{i\left(\omega_{Ir}^2 - f^2\right)}{ik\omega_{Ir} + fl}\hat{u} = \frac{i\left(\omega_{Ir}^2 - f^2\right)}{il\omega_{Ir} - fk}\hat{v}, \tag{B4}$$

$$\hat{w} = \frac{-\omega_{Ir}}{\left(N_B^2 - \omega_{Ir}^2\right)}\left(m - \frac{i}{2\mathcal{H}} + \frac{i}{\gamma\mathcal{H}}\right)\hat{p}, \tag{B5}$$

$$\hat{\rho} = \frac{\left[i\left(m - \frac{i}{2\mathcal{H}}\right)N_B^2 - \frac{\omega_{Ir}^2}{\gamma\mathcal{H}}\right]}{g\left(N_B^2 - \omega_{Ir}^2\right)}\hat{p}, \tag{B6}$$

$$\hat{T} = \frac{-N_B^2\left(im - \frac{1}{2\mathcal{H}}\right) + \frac{\omega_{Ir}^2}{\gamma\mathcal{H}}(1-\gamma)}{g\left(N_B^2 - \omega_{Ir}^2\right)}\hat{p}, \tag{B7}$$

$$\hat{w} = \frac{-\omega_{Ir}\left(m - \frac{i}{2\mathcal{H}} + \frac{i}{\gamma\mathcal{H}}\right)\left(\omega_{Ir}^2 - f^2\right)\left(k\omega_{Ir} + ifl\right)}{\left(N_B^2 - \omega_{Ir}^2\right)\left(k^2\omega_{Ir}^2 + f^2l^2\right)}\hat{u}, \tag{B8}$$

$$\hat{w} = \frac{-\omega_{Ir}\left(m - \frac{i}{2\mathcal{H}} + \frac{i}{\gamma\mathcal{H}}\right)\left(\omega_{Ir}^2 - f^2\right)\left(l\omega_{Ir} - ifk\right)}{\left(N_B^2 - \omega_{Ir}^2\right)\left(l^2\omega_{Ir}^2 + f^2k^2\right)}\hat{v}, \tag{B9}$$

$$\hat{w} = \frac{-g\omega_{Ir}\left(m - \frac{i}{2\mathcal{H}} + \frac{i}{\gamma\mathcal{H}}\right)}{i\left(m - \frac{i}{2\mathcal{H}}\right)N_B^2 - \frac{\omega_{Ir}^2}{\gamma\mathcal{H}}}\hat{\rho}, \tag{B10}$$

$$\hat{T} = \frac{N_B^2\left(im - \frac{1}{2\mathcal{H}}\right) - \frac{\omega_{Ir}^2}{\gamma\mathcal{H}}(1-\gamma)}{g\omega_{Ir}\left(m - \frac{i}{2\mathcal{H}} + \frac{i}{\gamma\mathcal{H}}\right)}\hat{w}. \tag{B11}$$

If the GWs and AWs are assumed to have the oscillatory form $e^{i(-\omega_r t + kx + ly + mz)}$ instead, then one must replace i by $-i$ in Equations (B3)–(B11) to obtain the corresponding compressible polarization relations. Equations (B3)–(B11) show that compressible effects are important for $|m|\mathcal{H} \ll 1$, or $|\lambda_z| \gg 2\pi\mathcal{H}$. In the limit that $f = 0$, it is easy to show that Equations (B8), (B10), and (B11) agree with the compressible, dissipative polarization relations derived in Vadas and Fritts (2005) (Equations (B1)–(B3) in that paper) in the limit that $\nu = 0$ (and for $i \to -i$). Note also that Equation (B4) agrees with Equation (27) in FA03. However, Equation (B5) differs significantly from Equation (28) in FA03 and also differs slightly from the correction to FA03 (Equation (28) in *Fritts and Alexander* [2012]). We believe that Equation (B5) is the correct expression.

[71] The Boussinesq limit occurs for GWs with $|\lambda_z| \ll 4\pi\mathcal{H}$, which is $|\lambda_z| \ll 90$ km in the lower atmosphere. In this limit, Equations (B3)–(B4) are the same, and Equations (B5)–(B11) reduce to the following:

$$\hat{w} = \frac{-\omega_{Ir}m}{\left(N_B^2 - \omega_{Ir}^2\right)}\hat{p}, \tag{B12}$$

$$\hat{\rho} = \frac{imN_B^2}{g\left(N_B^2 - \omega_{Ir}^2\right)}\hat{p}, \tag{B13}$$

$$\hat{T} = \frac{-imN_B^2}{g\left(N_B^2 - \omega_{Ir}^2\right)}\hat{p}, \tag{B14}$$

$$\hat{w} = \frac{-\omega_{Ir}m\left(\omega_{Ir}^2 - f^2\right)\left(k\omega_{Ir} + ifl\right)}{\left(N_B^2 - \omega_{Ir}^2\right)\left(k^2\omega_{Ir}^2 + f^2l^2\right)}\hat{u}, \tag{B15}$$

$$\hat{w} = \frac{-\omega_{Ir}m\left(\omega_{Ir}^2 - f^2\right)\left(l\omega_{Ir} - ifk\right)}{\left(N_B^2 - \omega_{Ir}^2\right)\left(l^2\omega_{Ir}^2 + f^2k^2\right)}\hat{v}, \tag{B16}$$

$$\hat{w} = \frac{ig\omega_{Ir}}{N_B^2}\hat{\rho}, \tag{B17}$$

$$\hat{T} = \frac{iN_B^2}{g\omega_{Ir}}\hat{w}. \tag{B18}$$

Note that Equations (B3), (B12), (B14), and (B17) agree with Equations (4), (C4), (C5), and (C3), respectively, in *Nicolls et al.* [2010] (for $i \to -i$ and using Equation (59)). Additionally, in the limit that $\omega_{Ir}^2 \ll N_B^2$, Equations (B15)–(B16) agree with Equations (C8)–(C9) in *Nicolls et al.* [2010], respectively.

Appendix C: Initial Condition Solutions

[72] In this appendix, we derive the initial value solutions (i.e., for no forces/heat/coolings, $F_x = F_y = F_z = J = 0$). We use the fact that the inverse transform of $\mathcal{L}(\widetilde{\psi})$ is

$$\widetilde{\psi}(t) = \frac{1}{2\pi i}\int e^{s_r t}\mathcal{L}\left(\widetilde{\psi}(s_r)\right)ds_r = \frac{1}{2\pi i}e^{i\left(k\overline{U}+l\overline{V}\right)t}\int e^{st}\mathcal{L}\left(\widetilde{\psi}(s)\right)ds, \tag{C1}$$

where we have used Equation (26), since $ds_r = ds$. We then solve Equations (16)–(20) with $\mathcal{F} = 0$. The compressible initial value solutions (denoted by the subscripts "IV") are

$$\begin{aligned}\widetilde{\xi}_{IV}(t) = e^{i\left(k\overline{U}+l\overline{V}\right)t}\Bigg[&\frac{i}{f^2-\omega_1^2}\left\{\left(\frac{lfE}{\omega_1} - k\omega_1 F\right)\sin\omega_1 t + (kE + lfF)\cos\omega_1 t\right\} \\ &+ \frac{i}{f^2-\omega_2^2}\left\{\left(\frac{lfG}{\omega_2} - k\omega_2 H\right)\sin\omega_2 t + (kG + lfH)\cos\omega_2 t\right\} + \frac{ilI}{f}\Bigg]\end{aligned} \tag{C2}$$

$$\begin{aligned}\widetilde{\sigma}_{IV}(t) = e^{i\left(k\overline{U}+l\overline{V}\right)t}\Bigg[&\frac{i}{f^2-\omega_1^2}\left\{-\left(\frac{kfE}{\omega_1} + l\omega_1 F\right)\sin\omega_1 t + (lE - kfF)\cos\omega_1 t\right\} + \frac{i}{f^2-\omega_2^2} \\ &\times\left\{-\left(\frac{kfG}{\omega_2} + l\omega_2 H\right)\sin\omega_2 t + (lG - kfH)\cos\omega_2 t\right\} - \frac{ikI}{f}\Bigg]\end{aligned} \tag{C3}$$

$$\begin{aligned}\widetilde{\eta}_{IV}(t) = e^{i\left(k\overline{U}+l\overline{V}\right)t}\left(im_s - \frac{1}{\gamma\mathcal{H}}\right)\Bigg\{&\frac{1}{N_B^2-\omega_1^2}\left(E\cos\omega_1 t - F\omega_1\sin\omega_1 t\right) \\ &+ \frac{1}{N_B^2-\omega_2^2}\left(G\cos\omega_2 t - H\omega_2\sin\omega_2 t\right)\Bigg\}\end{aligned} \tag{C4}$$

$$\begin{aligned}\widetilde{\phi}_{IV}(t) = e^{i\left(k\overline{U}+l\overline{V}\right)t}\Bigg[&\frac{\left(-\omega_1^2 + im_s(\gamma-1)g\right)}{c_s^2\left(N_B^2-\omega_1^2\right)}\left(\frac{E}{\omega_1}\sin\omega_1 t + F\cos\omega_1 t\right) \\ &+ \frac{\left(-\omega_2^2 + im_s(\gamma-1)g\right)}{c_s^2\left(N_B^2-\omega_2^2\right)}\left(\frac{G}{\omega_2}\sin\omega_2 t + H\cos\omega_2 t\right) + \frac{im_s}{g}I\Bigg]\end{aligned} \tag{C5}$$

$$\widetilde{\psi}_{IV}(t) = e^{i\left(k\overline{U}+l\overline{V}\right)t}\left[\frac{E}{\omega_1}\sin\omega_1 t + F\cos\omega_1 t + \frac{G}{\omega_2}\sin\omega_2 t + H\cos\omega_2 t + I\right], \tag{C6}$$

where

$$\epsilon = im_s g\widetilde{\psi}(0) + g\widetilde{\phi}(0)\delta \tag{C7}$$

$$E = \frac{1}{s_2^2 - s_1^2}\left[\delta\left(s_1^2 + f^2\right)\widetilde{\eta}(0) - ic_s^2\alpha\left(s_1^2 + N_B^2\right)\right] \tag{C8}$$

$$F = -\frac{1}{s_1^2\left(s_2^2 - s_1^2\right)}\left[(\widetilde{\psi}(0)s_1^2 + \epsilon)(s_1^2 + f^2) + ic_s^2\beta f\left(s_1^2 + N_B^2\right)\right] \tag{C9}$$

$$G = \frac{1}{s_2^2 - s_1^2}\left[-\delta(s_2^2 + f^2)\widetilde{\eta}(0) + ic_s^2\alpha\left(s_2^2 + N_B^2\right)\right] \tag{C10}$$

$$H = \frac{1}{s_2^2\left(s_2^2 - s_1^2\right)}\left[\left(\widetilde{\psi}(0)s_2^2 + \epsilon\right)\left(s_2^2 + f^2\right) + ic_s^2\beta f\left(s_2^2 + N_B^2\right)\right] \tag{C11}$$

$$I = \frac{f}{s_1^2 s_2^2}\left(f\epsilon + ic_s^2\beta N_B^2\right). \tag{C12}$$

It is then easy to show that Equations (C2)–(C6) reduce to Equations (B.1)–(B.5) in VF01.

[73] When $k = l = k_H = 0$, then $\omega_1 = f$ from Equation (31). This causes the denominators of the GW terms in Equations (C2) and (C3) to equal zero. Therefore, we calculate $\widetilde{\xi}_{IV}(t)$ and $\widetilde{\sigma}_{IV}(t)$ directly from Equations (16)–(17) in this special case, since the horizontal velocity perturbations decouple from the pressure, vertical velocity, and density perturbations:

$$\widetilde{\xi}_{IV}(t) = \widetilde{\sigma}(0)\sin ft + \widetilde{\xi}(0)\cos ft, \tag{C13}$$

$$\widetilde{\sigma}_{IV}(t) = -\widetilde{\xi}(0)\sin ft + \widetilde{\sigma}(0)\cos ft. \tag{C14}$$

Note that the Doppler frequency shift, $k\overline{U} + l\overline{V}$, is zero.

[74] When $k = l = k_H = 0$ and $f = 0$, then $\omega_1 = 0$. This causes the denominators of F and I to equal zero (see Equations (C9) and (C12)). In this special case, $\widetilde{\xi}_{IV}(t)$ and $\widetilde{\sigma}_{IV}(t)$ are given by Equations (C13)–(C14) with $f = 0$, and

$$\widetilde{\eta}_{IV}(t) = \frac{im_s - 1/(\gamma\mathcal{H})}{N_B{}^2 - \omega_2^2}\left(G'\cos\omega_2 t - H'\omega_2\sin\omega_2 t\right) \tag{C15}$$

$$\widetilde{\phi}_{IV}(t) = \frac{-\omega_2^2 + im_s(\gamma - 1)g}{c_s^2\left(N_B{}^2 - \omega_2^2\right)}\left(\frac{G'}{\omega_2}\sin\omega_2 t + H'\cos\omega_2 t\right) + \frac{im_s}{g}I' \tag{C16}$$

$$\widetilde{\psi}_{IV}(t) = \left(\frac{G'}{\omega_2}\sin\omega_2 t + H'\cos\omega_2 t\right) + I', \tag{C17}$$

where

$$G' = -\delta\widetilde{\eta}(0), \quad H' = \widetilde{\psi}(0) + \epsilon/s_2^2, \quad I' = -\epsilon/s_2^2. \tag{C18}$$

Appendix D: Special Case of the Forced/Heated Solutions

[75] In this appendix, we derive special cases of the forced/heated solutions. When $k = l = k_H = 0$, then $\omega_1 = f$ from Equation (31). This causes the denominators of Equations (40)–(41) and Equations (45)–(46) to equal zero. Therefore, we must calculate $\widetilde{\xi}_{FH}(t)$ and $\widetilde{\sigma}_{FH}(t)$ directly from Equations (16)–(17) in this special case, since the horizontal velocity perturbations decouple from the pressure, vertical velocity, and density perturbations. During the forcing (i.e., when $0 \le t \le \chi$), the solutions are

$$\widetilde{\xi}_{FH}(t) = \frac{\hat{a}^2}{\chi\left(\hat{a}^2 - f^2\right)}\left[\widetilde{F_{xs}}\left\{\frac{\sin ft}{f} - \frac{\sin\hat{a}t}{\hat{a}}\right\} + \frac{\widetilde{F_{ys}}}{f\hat{a}^2}\left\{\hat{a}^2(1 - \cos ft) + f^2\left(\cos\hat{a}t - 1\right)\right\}\right] \tag{D1}$$

$$\widetilde{\sigma}_{FH}(t) = \frac{\hat{a}^2}{\chi\left(\hat{a}^2 - f^2\right)}\left[\frac{\widetilde{F_{xs}}}{f\hat{a}^2}\left\{\hat{a}^2(\cos ft - 1) - f^2\left(\cos\hat{a}t - 1\right)\right\} + \widetilde{F_{ys}}\left\{\frac{\sin ft}{f} - \frac{\sin\hat{a}t}{\hat{a}}\right\}\right]. \tag{D2}$$

After the forcing (i.e., when $t \ge \chi$), the solutions are

$$\widetilde{\xi}_{FH}(t) = \frac{\hat{a}^2}{\chi f\left(\hat{a}^2 - f^2\right)}\left[\widetilde{F_{xs}}\mathcal{S}(f) - \widetilde{F_{ys}}\mathcal{C}(f)\right] \tag{D3}$$

$$\widetilde{\sigma}_{FH}(t) = \frac{\hat{a}^2}{\chi f\left(\hat{a}^2 - f^2\right)}\left[\widetilde{F_{xs}}\mathcal{C}(f) + \widetilde{F_{ys}}\mathcal{S}(f)\right]. \tag{D4}$$

If $k = l = k_H = 0$ and $f = 0$, then the denominators of Equations (D1)–(D4) equal zero. For this special case, the horizontal velocity solutions are simple. During the forcing (i.e., when $0 \le t \le \chi$), the solutions are

$$\widetilde{\xi}_{FH}(t) = \frac{\widetilde{F_{xs}}}{\chi}\left[t - \frac{\sin\hat{a}t}{\hat{a}}\right] \tag{D5}$$

$$\widetilde{\sigma}_{FH}(t) = \frac{\widetilde{F_{ys}}}{\chi}\left[t - \frac{\sin\hat{a}t}{\hat{a}}\right]. \tag{D6}$$

After the forcing (i.e., when $t \ge \chi$), the solutions are

$$\widetilde{\xi}_{FH}(t) = \widetilde{F_{xs}} \tag{D7}$$

$$\widetilde{\sigma}_{FH}(t) = \widetilde{F_{ys}}. \tag{D8}$$

When $k = l = k_H = 0$ and $f = 0$, then $s_1 = 0$. This causes K, O, and P to be ∞ from Equations (52), (55), and (56). In this case, $\widetilde{\eta}_{FH}(t)$, $\widetilde{\phi}_{FH}(t)$, and $\widetilde{\psi}_{FH}(t)$ are given by Equations (42)–(44) during the forcing/heating and by Equations (47)–(49) after the forcing/heating but with the following replacements: $K \to K'$, $M \to M'$, $N \to N'$, $O \to O'$, $P \to P'$, $Q \to Q'$, and $R \to R'$, where

$$K' = -\frac{im_s g\widetilde{J_s}}{\hat{a}^2 s_2^2}, \quad M' = \frac{\left(im_s g - \hat{a}^2\right)\widetilde{J_s}}{\hat{a}^2\left(\hat{a}^2 + s_2^2\right)}, \tag{D9}$$

$$N' = -\frac{\delta\widetilde{F_{zs}}}{\hat{a}^2\left(\hat{a}^2 + s_2^2\right)}, \quad O' = 0, \quad P' = 0, \tag{D10}$$

$$Q' = \frac{\left(im_s g + s_2^2\right)\widetilde{J_s}}{s_2^2\left(\hat{a}^2 + s_2^2\right)}, \quad R' = -\frac{\delta\widetilde{F_{zs}}}{s_2^2\left(\hat{a}^2 + s_2^2\right)}. \tag{D11}$$

[76] **Acknowledgments.** We would like to thank Michael Nicolls for checking the derivation of the compressible polarization relations in Appendix B and Erich Becker for clarifying the heat/cooling temperature tendencies caused by GW dissipation (see Equation (71)). This research was supported by NSF grants ATM-0537311, ATM-0836195, AGS-1139149, and AGS-1242616, and by NASA contracts NNH07CC81C, NNH08CE12C, NNH10CC98C, and NNH12CE58C.

References

Abramowitz, M., and I. A. Stegun (1972), *Handbook of Mathematical Functions*, Dover Publications, New York.

Alexander, M. J., J. R. Holton, and D. R. Durran (1995), The gravity wave response above deep convection in a squall line simulation, *J. Atmos. Sci.*, *52*(12), 2212–2226, doi:10.1175/1520-0469.

Becker, E. (2004), Direct heating rates associated with gravity wave saturation, *J. Atmos. Terr. Phys.*, *66*, 683–696.

Beres, J. H. (2004), Gravity wave generation by a three-dimensional thermal forcing, *J. Atmos. Sci.*, *61*, 1805–1815, doi:10.1175/1520-0469(2004)061<1805:GWGBAT>2.0.CO;2.

Bretherton, F. P. (1969), On the mean motion induced by internal gravity waves, *J. Fluid Mech.*, *36*, 785–803.

Choi, H.-J., H.-Y. Chun, and I.-S. Song (2007), Characteristics and momentum flux spectrum of convectively forced internal gravity waves in ensemble numerical simulations, *J. Atmos. Sci.*, *64* (10), 3723–3734, doi:10.1175/JAS4037.1.

Earle, G. D., A. Mwene-Musumba, and S. L. Vadas (2008), Satellite-based measurements of gravity wave-induced mid-latitude plasma density perturbations, *J. Geophys. Res.*, *113*, A03303, doi:10.1029/2007JA012766.

Fritts, D. C., and M. J. Alexander (2003), Gravity wave dynamics and effects in the middle atmosphere, *Rev. Geophys.*, *41*, 1003, doi:10.1029/2001RG000106.

Fritts, D. C., S. L. Vadas, K. Wan, and J. A. Werne (2006), Mean and variable forcing of the middle atmosphere by gravity waves, *J. Atmos. Solar-Terres. Phys.*, *68*, 247–265.

Fritts, D. C., and M. J. Alexander (2012), Correction to "Gravity wave dynamics and effects in the middle atmosphere", *Rev. Geophys.*, *50*, RG3004, doi:10.1029/2012RG000409.

Fritts, D. C., and S. Vadas (2008), Gravity wave penetration into the thermosphere: Sensitivity to solar cycle variations and mean winds, *Ann. Geophys.*, *26*, 3841–3861, doi:10.5194/angeo-26-3841-2008.

Hickey, M. P., and K. D. Cole (1987), A quartic dispersion equation for internal gravity waves in the thermosphere, *J. Atmos. Terres. Phys.*, *49*, 889–899.

Hines, C. O. (1960), Internal atmospheric gravity waves at ionospheric heights, *Can. J. Phys.*, *38*, 1441–1481.

Hines, C. O. (1965), Dynamical heating of the upper atmosphere, *J. Geophys. Res.*, *70*, 177–183, doi:10.1029/JZ070i001p00177.

Holton, J. R. (1992), *An Introduction to Dynamic Meteorology*, 507 pp., Academic Press, San Diego, Calif.

Holton, J. R., and M. J. Alexander (1999), Gravity waves in the mesosphere generated by tropospheric convection, *Tellus*, *51A-B*, 45–58.

Horinouchi, T., T. Nakamura, and J.-I. Kosaka (2002), Convectively generated mesoscale gravity waves simulated throughout the middle atmosphere, *Geophys. Res. Lett.*, *29*(21), 2007, doi:10.1029/2002GL016069.

Kundu, P. (1990), *Fluid Mechanics*, 638 pp., Academic Press, San Diego, Calif.

Lane, T. P., M. J. Reeder, and T. L. Clark (2001), Numerical modeling of gravity waves generated by deep tropical convection, *J. Atmos. Sci.*, *58*, 1249–1274, doi:10.1175/1520-0469(2001)058<1249:NMOGWG>2.0.CO;2.

Lane, T. P., R. D. Sharman, T. L. Clark, and H.-M. Hsu (2003), An investigation of turbulence generation mechanisms above deep convection, *J. Atmos. Sci.*, *60*, 1297–1321, doi:10.1175/1520-0469.

Lane, T. P., and J. C. Knievel (2005), Some effects of model resolution on simulated gravity waves generated by deep, mesoscale convection, *J. Atmos. Sci.*, *62*, 3408–3419, doi:10.1175/JAS3513.1.

Lane, T. P., and R. D. Sharman (2006), Gravity wave breaking, secondary wave generation, and mixing above deep convection in a three-dimensional cloud model, *Geophys. Res. Lett.*, *33*, L23813, doi:10.1029/2006GL027988.

Larsen, M. F., W. E. Swartz, and R. F. Woodman (1982), Gravity-wave generation by thunderstorms observed with a vertically-pointing 430 MHz radar, *Geophys. Res. Lett.*, *9*(5), 571–574.

Lastovicka, J. (2006), Forcing of the ionosphere by waves from below, *J. Atmos. Solar Terres. Phys.*, *68*, 479–497.

Liu, H.-L. (2000), Temperature changes due to gravity wave saturation, *J. Geophys. Res.*, *105*, 12329–12336.

Makela, J. J., S. L. Vadas, R. Muryanto, T. Duly, and G. Crowley, (2010), Periodic spacing between consecutive equatorial plasma bubbles, *Geophys. Res. Lett.*, *37*, L14103, doi:10.1029/2010GL043968.

Marks, C. J., and S. D. Eckermann (1995), A three-dimensional nonhydrostatic ray-tracing model for gravity waves: Formulation and preliminary results for the middle atmosphere, *J. Atmos. Sci.*, *52*, 1959–1984.

Nicolls, M. J., R. H. Varney, S. L. Vadas, P. A. Stamus, C. J. Heinselman, R. B. Cosgrove, and M. C. Kelley (2010), Influence of an inertia-gravity wave on mesospheric dynamics: A case study with the Poker Flat Incoherent Scatter Radar, *J. Geophys. Res.*, *115*, D00N02, doi:10.1029/2010JD014042.

Pandya, R. E., and M. J. Alexander (1999), Linear stratospheric gravity waves above convective thermal forcing, *J. Atmos. Sci.*, *56* (14), 2434–2446.

Piani, C., D. Durran, M. J. Alexander, and J. R. Holton (2000), A numerical study of three dimensional gravity waves triggered by deep tropical convection, *J. Atmos. Sci.*, *57*, 3689–3702.

Pitteway, M. L. V., and C. O. Hines (1963), The viscous damping of atmospheric gravity waves, *Can. J. Phys.*, *41*, 1935–1948.

Richmond, A. D. (1978), Gravity wave generation, propagation, and dissipation in the thermosphere, *J. Geophys. Res.*, *83*, 4131–4145.

Roble, R. G., and E. C. Ridley (1994), A thermosphere-ionosphere-mesosphere-electrodynamics general circulation model (TIME-GCM): equinox solar cycle minimum simulations (30-500 km), *Geophys. Res. Lett.*, *21*, 417–420.

Song, I.-S., H.-Y. Chun, and P. P. Lane (2003), Generation mechanisms of convectively forced internal gravity waves and their propagation to the stratosphere, *J. Atmos. Sci.*, *60*, 1960–1980, doi:10.1175/1520-0469(2003)060<1960:GMOCFI>2.0.CO;2.

Stull, R. B. (1976), Internal gravity waves generated by penetrative convection, *J. Atmos. Sci.*, *33*(7), 1279–1286.

Vadas, S. L., and D. C. Fritts (2001), Gravity wave radiation and mean responses to local body forces in the atmosphere, *J. Atmos. Sci.*, *58*, 2249–2279, doi:10.1175/1520-0469(2001)058<2249:GWRAMR>2.0.CO;2.

Vadas, S. L., D. C. Fritts, and M. J. Alexander (2003), Mechanism for the generation of secondary waves in wave breaking regions, *J. Atmos. Sci.*, *60*, 194–214, doi:10.1175/1520-0469(2003)060<0194:MFTGOS>2.0.CO;2.

Vadas, S. L, and D. C. Fritts (2004), Thermospheric responses to gravity waves arising from mesoscale convective complexes, *J. Atmos. Solar Terres. Phys.*, *66*, 781–804.

Vadas, S. L., and D. C. Fritts (2006), Influence of solar variability on gravity wave structure and dissipation in the thermosphere from tropospheric convection, *J. Geophys. Res.*, *111*, A10S12, doi:10.1029/2005JA011510.

Vadas, S. L. (2007), Horizontal and vertical propagation and dissipation of gravity waves in the thermosphere from lower atmospheric and thermospheric sources, *J. Geophys. Res.*, *112*, A06305, doi:10.1029/2006JA011845.

Vadas, S. L., and D. C. Fritts (2009), Reconstruction of the gravity wave field from convective plumes via ray tracing, *Ann. Geophys.*, *27*, 147–177, doi:10.5194/angeo-27-147-2009.

Vadas, S. L., M. J. Taylor, P.-D. Pautet, P. A. Stamus, D. C. Fritts, H.-L. Liu, F. T. Sao Sabbas, V. T. Rampinelli, P. Batista, and H. Takahashi (2009a), Convection: The likely source of the medium-scale gravity waves observed in the OH airglow layer near Brasilia, Brazil, during the SpreadFEx campaign, *Ann. Geophys.*, *27*, 231–259, doi:10.5194/angeo-27-231-2009.

Vadas, S. L., J. Yue, C.-Y. She, P. A. Stamus, and A. Liu (2009b), A model study of the effects of winds on concentric rings of gravity waves from a convective plume near Fort Collins on 11 May 2004, *J. Geophys. Res.*, *114*, D06103, doi:10.1029/2008JD010753.

Vadas, S. L., and H.-L. Liu (2009), The generation of large-scale gravity waves and neutral winds in the thermosphere from the dissipation of convectively-generated gravity waves, *J. Geophys. Res.*, *114*, A10310, doi:10.1029/2009JA014108.

Vadas, S. L., and G. Crowley (2010), Sources of the traveling ionospheric disturbances observed by the ionospheric TIDDBIT sounder near Wallops Island on October 30, 2007, *J. Geophys. Res.*, *115*, A07324, doi:10.1029/2009JA015053.

Vadas, S. L., and H.-L. Liu (2011), Neutral winds and densities at the bottomside of the F layer from primary and secondary gravity waves from deep convection, in *Aeronomy of the Earth's Atmosphere and Ionosphere.* IAGA Special Sopron Book Series, vol. 2, edited by M. A. Abduc, D. Pancheva, and A. Bhattacharyya, pp. 131–139, Springer, New York.

Vadas, S. L., and H.-L. Liu (2013), Numerical modeling of the large-scale neutral and plasma responses to the body forces created by the dissipation of gravity waves from 6 hours of deep convection in Brazil, *J. Geophys. Res.*, doi:10.1002/jgra.50249, in press.

Vadas, S. L., J. Yue, and T. Nakamura (2012), Mesospheric concentric gravity waves generated by multiple convection storms over the North America Great Plain, *J. Geophys. Res.*, *117*, D7, doi:10.1029/2011JD017025.

Vadas, S. L., and M. J. Nicolls (2012), The phases and amplitudes of gravity waves propagating and dissipating in the thermosphere: Theory, *J. Geophys. Res.*, *117*, A05322, doi:10.1029/2011JA017426.

Vadas, S. L., and D. C. Fritts (2013), Correction to "Gravity wave radiation and mean responses to local body forces in the atmosphere, *J. Atmos. Sci.*, in press.

Walterscheid, R. L. (1981), Dynamical cooling induced by dissipating internal gravity-waves, *J. Geophys. Res.*, *8*, 1235–1238, doi:10.1029/GL008i012p01235.

Walterscheid, R. L., G. Schubert, and D. G. Brinkman (2001), Small-scale gravity waves in the upper mesosphere and lower thermosphere generated by deep tropical convection, *J. Geophys. Res.*, *106*, D23, 31825–31832, doi:10.1029/2000JD000131.
Yiğit, E., and A. S. Medvedev (2009), Heating and cooling of the thermosphere by internal gravity waves, *Geophys. Res. Lett.*, *36*, L14807, doi: 10.1029/2009GL038507.
Zhu, X., and J. R. Holton (1987), Mean fields induced by local gravity-wave forcing in the middle atmosphere, *J. Atmos. Sci.*, *44*, 620–630.